Laser-based Optical Diagnostics of Electrode Wear

A Pioneering Work

Zhang, Kailun

2025

Document Version:
Publisher's PDF, also known as Version of record

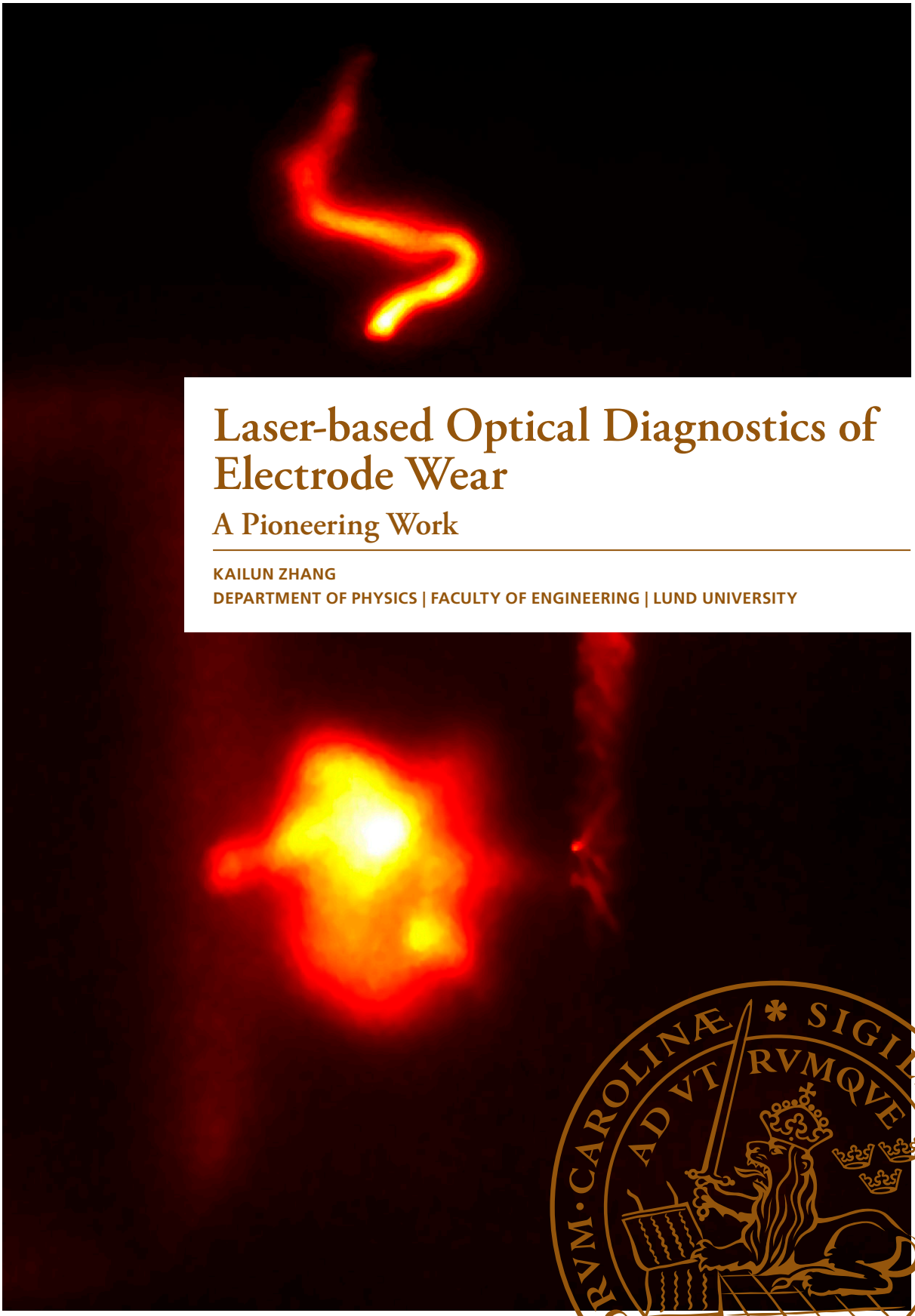

Laser-based Optical Diagnostics of Electrode Wear

A Pioneering Work

KAILUN ZHANG
DEPARTMENT OF PHYSICS | FACULTY OF ENGINEERING | LUND UNIVERSITY

Laser-based Optical Diagnostics of Electrode Wear

Laser-based Optical Diagnostics of Electrode Wear

A Pioneering Work

by Kailun Zhang

LUND
UNIVERSITY

Thesis for the degree of Doctor of Philosophy in Engineering

Thesis advisors: Prof. Dr. Mattias Richter
Assoc. Prof. Dr. Andreas Ehn

Faculty opponent: Assoc. Prof. Dr. Iain Burns

To be presented, with the permission of the Division of Combustion Physics of Lund University, for public criticism in the Rydberg lecture hall (Mötesplats Rydberg) at the Department of Physics on Friday, the 12nd of September 2025 at 9:15 a.m.

Organization	Document name
LUND UNIVERSITY Department of Physics Box 118 SE – 221 00 LUND Sweden	**DOCTORAL DISSERTATION** Date of disputation 2025 - 09 - 12 Sponsoring organization
Author(s) Kailun Zhang	

Title and subtitle

Laser-based Optical Diagnostics of Electrode Wear: A Pioneering Work

Abstract

Improving spark-ignition engines in terms of efficiency and compatibility with renewable fuels is essential for ensuring energy security, cost-effectiveness, and sustainability. However, electrode wear of spark plugs, especially under conditions involving novel fuels and lean mixtures, becomes a significant technical challenge. Therefore, a deeper understanding of the interactions between spark discharges and electrode materials is more crucial than ever.

Conventional *ex-situ*, long-term testing methods lack the temporal and spatial resolution required to capture the dynamics of electrode wear during short spark discharges. As a pioneering work, this thesis incorporates laser-based optical diagnostics to study electrode wear of spark plugs *in-situ* for the first time.

Strong nickel emission lines were detected between two prominent nitrogen bands during spark discharges. Several excitation pathways of nickel atoms were investigated, identifying the 336.96 nm line as the optimal transition for diagnostic purposes. The effective fluorescence lifetime of nickel under atmospheric conditions was measured for the first time and found to be approximately 1.1 ns, with no statistically significant variation throughout the discharge duration. The spatiotemporal behavior of gas-phase nickel atoms originating from the spark plug electrodes was characterized using planar laser-induced fluorescence. The spatial distribution of nickel atoms across the electrode gap varied with pressure, indicating different wear mechanisms. Spark power was identified as the dominant factor driving electrode erosion via evaporation, and a classic model was modified accordingly.

Overall, this thesis provides valuable experimental data and offers new insights into the fundamental mechanisms governing spark discharge-electrode interactions, contributing to the advancement of ignition systems for future spark ignition internal combustion engines.

Key words

Spark Discharge, Electrode Wear, Laser Diagnostics, Optical Emission Spectroscopy, Laser-induced Fluorescence, Spark Plug, Nickel

Classification system and/or index terms (if any)

Supplementary bibliographical information	Language
	English
ISSN and key title	ISBN
	978-91-8104-507-9 (Print) 978-91-8104-508-6 (Online)
Recipient's notes	Number of pages: 164 / Price
	Security classification

Laser-based Optical Diagnostics of Electrode Wear

A Pioneering Work

by Kailun Zhang

LUND
UNIVERSITY

A doctoral thesis at a university in Sweden takes either the form of a single, cohesive research study (monograph) or a summary of research papers (compilation thesis), which the doctoral student has written alone or together with one or several other author(s).

In the latter case the thesis consists of two parts. An introductory text puts the research work into context and summarizes the main points of the papers. Then, the research publications themselves are reproduced, together with a description of the individual contributions of the authors. The research papers may either have been already published or are manuscripts at various stages (in press, submitted, or in draft).

Faculty Opponent:	**Assoc. Prof. Dr. Iain Burns** University of Strathclyde, Scotland, UK
Evaluation Committee:	**Prof. Dr. Knut Deppert** Lund University, Sweden **Assoc. Prof. Dr. Hampus Nilssson** Malmö University, Sweden **Dr. Raymond Reinmann** Scania AB, Sweden

Funding information: The thesis work was financially supported by Swedish Energy Agency through Fordonsstrategisk Forskning och Innovation (FFI, No. 50180-1).

Cover illustration front: Upper: Spark-produced plasma emission within the spark plug gap. Lower: Laser-induced nickel fluorescence within the spark plug gap.
Cover illustration back: The handmade slit used to block the stray light in the pressurized cell.

Division of Combustion Physics, Department of Physics

ISBN: 978-91-8104-507-9 (Print)
ISBN: 978-91-8104-508-6 (Online)

Printed in Sweden by Media-Tryck, Lund University, Lund 2025

Dedicated to my parents
Ruili Zhao & Sibao Zhang

献给我的父母
赵蕊莉 & 张四宝

Start of the journey.

@ Mensa der Ruhr-Universität Bochum

Seeing is believing

眼见为实

Table of Contents

Abstract

Improving spark-ignition engines in terms of efficiency and compatibility with renewable fuels is essential for ensuring energy security, cost-effectiveness, and sustainability. However, electrode wear of spark plugs, especially under conditions involving novel fuels and lean mixtures, becomes a significant technical challenge. Therefore, a deeper understanding of the interactions between spark discharges and electrode materials is more crucial than ever.

Conventional *ex-situ*, long-term testing methods lack the temporal and spatial resolution required to capture the dynamics of electrode wear during short spark discharges. As a pioneering work, this thesis incorporates laser-based optical diagnostics to study electrode wear of spark plugs *in-situ* for the first time.

Strong nickel emission lines were detected between two prominent nitrogen bands during spark discharges. Several excitation pathways of nickel atoms were investigated, identifying the 336.96 nm line as the optimal transition for diagnostic purposes. The effective fluorescence lifetime of nickel under atmospheric conditions was measured for the first time and found to be approximately 1.1 ns, with no statistically significant variation throughout the discharge duration. The spatiotemporal behavior of gas-phase nickel atoms originating from the spark plug electrodes was characterized using planar laser-induced fluorescence. The spatial distribution of nickel atoms across the electrode gap varied with pressure, indicating different wear mechanisms. Spark power was identified as the dominant factor driving electrode erosion via evaporation, and a classic model was modified accordingly.

Overall, this thesis provides valuable experimental data and offers new insights into the fundamental mechanisms governing spark discharge-electrode interactions, contributing to the advancement of ignition systems for future spark ignition internal combustion engines.

List of Papers

This thesis is based on the following papers, referred to by their Roman numerals:

I **Detection of Nickel Atoms Released from Electrodes in Spark Discharges Using Laser-Induced Fluorescence**

K. Zhang, R. Bi, J. Tidholm, J. Ängeby, M. Richter, A. Ehn
Applied Spectroscopy, Volume 79, Issue 2, pp. 281–288 (2025)
DOI: 10.1177/00037028241285150

II **Effective lifetime of Ni laser induced fluorescence excited at 336.9 nm during spark plug discharge**

R. Bi, **K. Zhang**, A. Ehn, M. Richter
Applied Physics B: Lasers and Optics, Volume 130, No. 147 (2024)
DOI: 10.1007/s00340-024-08279-w

III **Robust Ignition and Sparkplug Wear for H_2 SI-ICE**

J. Ängeby, **K. Zhang**, A. Johnsson, J. Tidholm, M. Richter, A. Ehn
Proceedings of 6th International Conference on Ignition Systems for SI Engines & 7th International Conference on Knocking in SI Engines, pp. 81–94 (2024)
DOI: 10.24053/9783381129928

IV **Investigation of Electrode Wear during Spark Discharges using Planar Laser-induced Fluorescence**

K. Zhang, H. Feuk, J. Ängeby, A. Ehn, M. Richter
Manuscript Submitted

Work about plasma-assited combustion not included in the thesis:

A **Single-shot 2D and 3D Imaging of Gas Discharge with Structured Laser Illumination**

Y. Bao, **K. Zhang**, C. Kong, E. Kristensson, A. Ehn
Proceedings of XXIII International Conference on Gas Dischargs and their Applications, pp. 392–395 (2023)

B **A Comprehensive Study on Dynamics of Flames in a Nanosecond Pulsed Discharge. Part I: Discharge Formation and Gas Heating**

Y. Bao, **K. Zhang**, J. Sun, T. Hurtig, A.A. Konnov, M. Richter, E. Kristensson, A. Ehn
Combustion and Flame, Volume 275, No. 114075 (2025)
DOI: 10.1016/j.combustflame.2025.114075

C **A Comprehensive Study on Dynamics of Flames in a Nanosecond Pulsed Discharge. Part II: Plasma-Assisted Ammonia and Methane Combustion**

J. Sun, Y. Bao, **K. Zhang**, A.A. Konnov, M. Richter, E. Kristensson, A. Ehn
Combustion and Flame, Volume 275, No. 114076 (2025)
DOI: 10.1016/j.combustflame.2025.114076

D **Spatiotemporal Imaging of NH_2 in Plasma-Assisted NH_3 Combustion via Nanosecond Pulsed Discharge**

J. Sun, **K. Zhang**, Y. Bao, C. Brackmann, M. Richter, A.A. Konnov, A. Ehn
Manuscript Submitted

Popular Summary

A significant milestone in the progress of human civilization and social development is the use of fire. Nowadays, more than 80% of human energy supply still comes from the combustion of fossil fuels (such as coal, oil, and natural gas). In the field of transportation, this proportion is even higher, exceeding 95%. However, the carbon dioxide produced during the combustion of fossil fuels accelerates global warming and the climate crisis, threatening all humans. Furthermore, considering the geographical differences between countries and regions, and the potential geopolitical risks arising from these differences, the security, cost, and sustainability of energy have always been and will continue to be the focus of scientists and engineers in various countries in the foreseeable future.

Although the use of renewable energy (such as solar, wind, and hydro power) has been increasing year by year, and in some countries and regions (such as the Nordic countries where the author resides), it has even become the main source of electricity supply, global replacement of fossil fuels is still a long way to go due to geographical and technological limitations. Therefore, the modification of existing infrastructure has become a quick and relatively inexpensive option. For example, in transportation and power generation, modifying existing internal combustion engine units to be compatible with eco-friendly fuels (such as hydrogen) has become a potential solution. Undoubtedly, such adaptations will bring some accompanying issues, such as pre-ignition and knocking. But surprisingly, compared to the vast and complex system, the electrode wear of small spark plugs used for ignition is the first issue needs to be solved.

With the invention and utilization of internal combustion engines in the mid-19th century, the electric spark plug used for ignition was also invented in 1860 and has since developed alongside internal combustion engines. Spark discharge can be approximated as a form of micro lightning, where gas is ionized in a very short time (on the order of 10^{-9} seconds), and collisions between particles generate high-temperature plasma, thus igniting the mixture of gases in the combustion chamber of the internal combustion engine. It can be imagined that, just like lightning causing damage to surface objects, sparks also damage the surface of the metal electrodes. Of course, such damage has attracted attention since

the invention of the spark plug, and various hypotheses and theories have been proposed. Moreover, compared to traditional fuels, experiments with hydrogen-oxygen mixtures show that wear on the metal electrodes of the spark plug accelerates significantly, shortening their lifespan, increasing maintenance frequency, downtime, and potentially causing engine misfires and even damage. We know that this wear involves the metal or alloy material leaving the surface of the electrode in some way, but the instantaneous nature of spark discharge and the strong background radiation from the plasma makes it difficult for commonly used offline diagnostic techniques and regular optical methods to characterize this wear phenomenon during spark discharge.

Laser-based advanced optical diagnostic techniques, due to their high temporal and spatial resolution, have been widely applied in research areas such as combustion and plasma. Inspired by this, the main focus of this thesis is to apply these techniques to investigate the interaction between spark discharge and its electrodes. For the first time, clear imaging of atomic clusters between the two spark plug electrodes has been achieved. We believe that the results of the thesis will help to improve the design of current electric ignition systems, extend the service life of commercial spark plugs, and refine existing theoretical models. Moreover, the strategies and methods presented in this work can be further extended to research on gas discharges and material interactions in other contexts.

科普简介

人类文明进步和社会发展的重要标志就是对于火的使用。直至今日，人类能源供应的百分之八十仍然来自于化石燃料（比如煤炭，石油和天然气）的燃烧。如果将目光聚焦在交通运输领域，该比例甚至高于百分之九十五。但是，由于化石能源燃烧过程中所产生的二氧化碳，导致了全球变暖的加速和气候危机，威胁着我们所有人类的生产和生活。不仅如此，考虑到各个国家和地区的地理差别和因此带来的潜在地缘政治风险，能源的安全、成本和可持续一直以来以及在可预见的未来都将会是各个国家科学家和工程师们努力的方向。

尽管最近可再生能源（比如太阳能，风能和水力）的使用比例在逐年提高，在某些国家和地区（比如作者身处的北欧地区）甚至已经成为电力供应的主要来源，但由于地理和现有技术的限制，对化石能源的全球性替代仍然有很长的一段路要走。因此对现存基础设施的改造成为了一个快速且成本相对低廉的选项，比如，在交通运输和电力生产领域，对现有的内燃机组进行环保燃料（例如氢气）的适配性改造。毋庸置疑，这样的适配会产生一些附带问题，比如提前点火和爆震。但不可置信的是，相对于复杂庞大的整个系统，用于引燃的小巧的火花塞的电极磨损将会是第一个需要解决的问题。

伴随着 19 世纪中叶内燃机的发明与利用，用于引燃的电火花塞也随之发明于 1860 年，并自从那时起就与内燃机一同发展。火花放电可以近似看作为一种微型闪电，气体在短时间（10^{-9} 秒量级）之内被击穿，各种粒子之间碰撞产生了高温等离子体，从而引燃了内燃机燃烧室内的混合气体。可以想像，就像闪电对地表物体的损害一样，火花也会破坏金属电极的表面。当然，这样的损伤自其发明那时起就引起了人们的注意，并随之有一些假设和理论被提出。而且，相比于传统燃料，在氢氧混合气的点火实验中发现，火花塞金属电极的磨损会大大加速，缩短了其使用寿命，增加了保养维护的频率和停机时间，甚至可能导致内燃机的失火和损坏。我们知道这种磨损是金属或者合金材料以某种方式离开了电极的表面，但火花放电的瞬时性和等离子体的强背景辐射，导致常用的离线诊断技术和普通光学手段无法对火花放电过程中所导致的磨损进行表征。

因具有出色的时间与空间分辨能力，基于激光的先进光学诊断技术被广泛应用于燃烧和等离子体等研究领域。受此启发，本文的工作聚焦于将该技术应用于研究火花放电与其电极之间的相互作用，并首次清晰成像了火花塞两电极之间的原子团。我们相信，本文的结论将有助于优化现有电点火系统的设计，延长商用火花塞的寿命，并进一步完善已有理论模型。此外，借助本文提出的策略和方法，该类先进光学诊断技术还可进一步拓展至其他涉及气体放电和物质相互作用的研究领域。

List of Abbreviations

- **CCD** – Charge-Coupled Device
- **CMOS** – Complementary Metal-Oxide-Semiconductor
- **FWHM** – Full Width at Half Maximum
- **ICE** – Internal Combustion Engine
- **ICP-OES** – Inductively Coupled Plasma Optical Emission Spectroscopy
- **LIF** – Laser-induced Fluorescence
- **MCP** – Micro-Channel Plate
- **MCU** – Master Control Unit
- **NIST** – National Institute of Standards and Technology of U.S.
- **OES** – Optical Emission Spectroscopy
- **OPA** – Optical Parametric Ampfilier
- **OPG** – Optical Parametric Generator
- **OPO** – Optical Parametric Oscillator
- **PLIF** – Planar Laser-induced Fluorescence
- **PMT** – Photomultiplier Tube
- **SI-ICE** – Spark-ignition Internal Combustion Engine
- **SNR** – Signal to Noise Ratio

List of Nomenclature

- T_b – Boiling temperature
- A – Einstein coefficient for spontaneous emission
- ε – Emissivity
- ΔH_{fus} – Enthalpy of fusion
- q – Heat conduction rate
- T_m – Melting temperature
- r – Heat radiation rate
- W_{spark} – Spark energy
- u – Spark voltage
- c_l – Specific heat of electrode in liquid state
- σ – Stefan-Boltzmann constant
- a – Thermal diffusivity
- ϱ – Density of electrode
- eV – Electron volt
- E_v – Energy for evaporation
- ΔH_{vap} – Enthalpy of vaporization
- m – Mass
- τ – Radiation lifetime
- i – Spark current
- P_{spark} – Spark power
- c – Specific heat
- c_s – Specific heat of electrode in solid state
- k – Thermal conductivity
- S – Total area of hot spots

Laser-based Optical Diagnostics of Electrode Wear

Chapter I

Introduction

Before I came here, I was confused about this subject.
Having listened to your lecture, I am still confused,
but on a higher level.

— Enrico Fermi

A defining feature of human civilization has long been the controlled use of fire - a fundamental form of combustion. From prehistoric times to the present day, combustion has provided essential benefits including processed food, warmth, light, and protection. Nowadays and in the foreseeable future, this principle will remain central, for example, in the sectors of electricity generation and transportation [1, 2]. Seen in Fig. 1.1 [1.1], more than 80% of the total energy of the whole world is supplied by the combustion of fossil fuels and the importance becomes more self-evident in the field of transportation. These facts indicate that further research about combustion is strongly demanded and necessary.

Energy security, affordablity & sustainablity

Recently, concerns have been raised regarding the global energy supply chain due to geographical disparities and potential geopolitical risks [3–6]. For Sweden, only 71,7% of the total energy demand is met through domestic production [7]. For the whole European Union, the situation is even more pronounced, with an energy imports dependency rate of 58% [8]. Needless to say, energy security is a critical concern for every country and region. Local energy production from renewable sources offers a viable alternative [9], which not only enhancing the immedicy but also reducing the risks of energy supply.

The cost of energy is another important factor to consider. Some sources, such as solar, hydro, and wind power, are relatively low-cost. However, due to the substantial investment

[1.1] The figure is made based on the open source data from International Energy Agency.

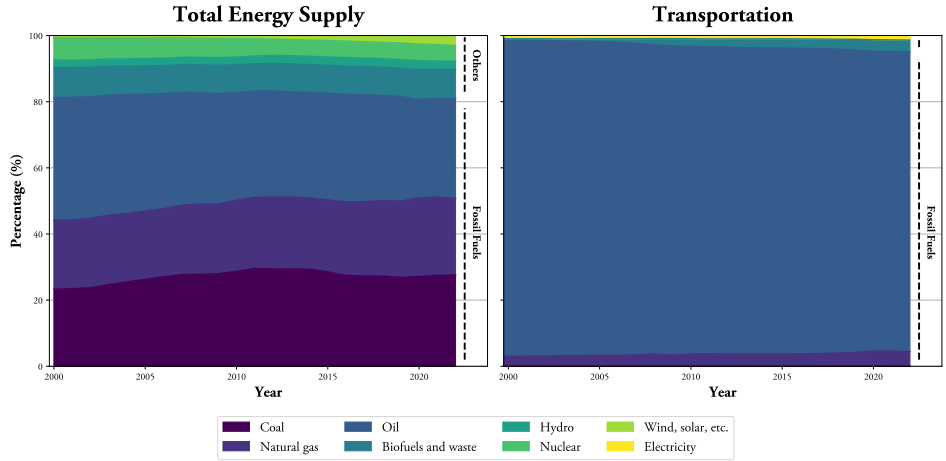

Figure 1.1: **Left:** Total energy supply by different sources in the whole world. **Right:** Consumption in the field of transportation by different sources.

required for infrastructure and the intermittent nature of these sources, combustible renewable fuels can serve as a practical substitute. Certain renewable fuels, such as ammonia, can serve as effective means of energy storage, which help alleviate pressure on the power grid [10, 11]. In the transportation sector, hydrogen SI-ICE can leverage existing manufacturing infrastructure and rely on widely available materials, making large-scale deployment more feasible [12–15]. Moreover, those engines are relatively inexpensive compared to other emerging propulsion technologies, such as fuel cells [16].

Last but not least, environmental concerns are escalating. Global warming, which is driven primarily by greenhouse gas emissions, poses an existential threat. According to international climate targets, the average increase in global temperature must be limited to 1.5 °C by the end of the 21st century to avoid catastrophic environmental consequences [17, 18]. The energy transtion and global emissions reduction need to be sped up.

In response to abovementioned reasons, the continuous development of ICE are necessary and one of the major transitions focuses on the adaption to renewable fuels, such as hydrogen (H_2) and ammonia (NH_3).

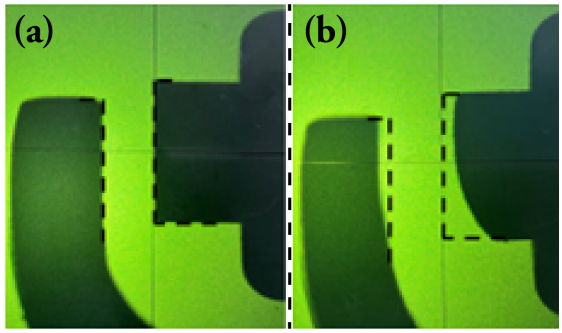

Figure 1.2: **(a):** A J-gap spark plug before long-term test. **(b):** The same spark plug after 52 millions sparks. The black dashed lines mark the original outline of the electrodes.

Key role of electrode wear in such large framwork

Despite the vision is promising, it can be imagined that there are technical challenges [19–23]. One of the such challenges is the accelerated electrode wear, which becomes a limiting factor in the lifetime of spark plugs, especially in demanding applications like lean-burn gas engines where high spark energy is required [24, 25]. As an example, commercial spark plugs used for fossil fuels last more than 1000 working hours [26]. While, when ignite hydrogen/air mixture, they will be worn out quickly and the lifespan decreases to a level far below the demand of customers [16, 27]. Consequently, the frequent need for spark plug replacement not only increases maintenance costs [1.2] but also poses a risk of unplanned downtime.

Undoubtedly, many efforts have been made to understand such electrode wear since the invention of the first commerically viable electric ignition system and spark plugs in the early 20th century [28]. These studies have primarily relied on long-term durability testing and involved visual inspections and post-mortem analyses to evaluate material loss and surface changes over time [29–40]. Fig. 1.2 [1.3] is an example showing such conventional methodology, which is a comparison of the volume between a new J-gap sparkplug before long-term test and after 52 million sparks. However, the degradation of electrodes occurs incrementally during each individual spark event, which lasts only tens to thousands of microseconds (μs). In order to understand the mechanisms and reveal the interactions between spark discharge and electrode, diagnostic tools with high temporal and spatial resolution, which have the ability to capture rapid, transient phenomena, is therefore crucial.

[1.2] Trust me, the cost for spark plug itself is way more expensive than you thought, not even considering the number of cylinders.

[1.3] The figure is re-made from Figure 5 in **Paper III**.

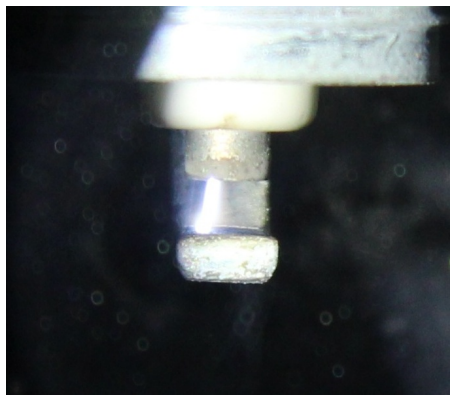

Figure 1.3: A close-up photograph of a spark plug during discharge.

Uniqueness of laser diagnostics

From spark plug to lightning, spark is an electrically conductive channel abruptly created through a insulating medium [41]. Fig. 1.3 is a photograph of a spark plug captured during a discharge. The intense plasma emission within the narrow electrode gap significantly hinders the accurate diagnosis of electrode wear, thereby necessitating the need for advanced techniques. Laser-based optical diagnostic methods are well-proved for the detection of target species in harsh environments, such as plasma and combustion [42–50]. Their non-intrusive nature and high spatiotemporal resolution make them ideally suitable for investigating the complex and instantaneous phenomena - spark-induced electrode wear.

Overview and structure of the thesis

The main objective of this thesis is to develop and apply laser-based optical diagnostic techniques for *in-situ* investigations on sparkplug wear and advance the funamental understanding of the interaction between spark discharge and electrode. The content is structured as follows:

• **Chapter II** introduces the fundamental physics of spark discharge and highlights the existing research gap of spark-induced electrode wear.

• **Chapter III** desrcibes the necessary initial spectral study in an obscure field for performing laser diagnostics from a practical perspective and establishes the cornerstone for subsequent LIF studies.

• **Chapter IV** presents the key findings of electrode wear by different mechanisms during spark discharges using LIF.

• **Chapter V** concludes the thesis with a comprehensive summary and an outlook on future research directions.

Chapter II

Let there be sparks

The first high-voltage magneto and spark plug [Picture: Bosch]

From the crackling sound when taking off clothes in dry days to one of the most beautiful and dangerous natural phenomenon – lightning, spark discharge is the very special one among all different kinds of gas discharges. In this chapter, the fundament of spark discharge will be presented with its distinct phases. The most common applications of spark discharge, as the ignition tool in SI-ICEs, will be introduced. Lastly, the interaction bewtween sparks and electrodes and current research status are given, which reveal the reasons for the demand of laser-based optical diagnostic methods.

2.1 Spark discharge

Spark discharge can be viewed in several phases - from the initial pre-breakdown events through the breakdown of gas, arc, glow, and their transitions [51]. Illustrated with a standard DC spark in Fig. 2.1, each phase has distinct characteristics in terms of voltage, current, and plasma-electrode interactions, which in turn influence how the electrodes are eroded by the spark. An brief overview of these phases is introduced here.

2.1.1 Pre-breakdown Phase

Before the main spark 'breakdown' occurs, there is a pre-breakdown stage. A detailed voltage-current waveform of this phase can be seen in Fig. 2.2 before the marked gas breakdown moment. In this stage, as the circuit is triggered to stop charging the ignition coil, the voltage across the spark plug gap rises rapidly [2.1] but no visible spark is present yet. Free

[2.1] Faraday's Law of Induction

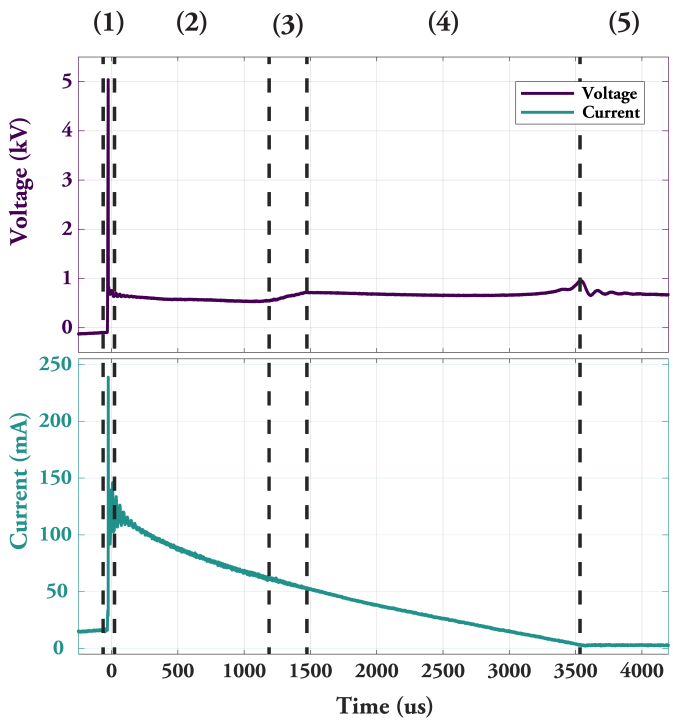

Figure 2.1: **The voltage and current characteristic waveform of a standard DC spark discharge, measured in atmospheric condition across a 1.2 mm gap.**
Different phases are marked with black dashed lines and numbers above the figure.
(1) Pre-breakdown and breakdown. (2) Arc phase. (3) Arc-glow transition. (4) Glow phase. (5) End of discharge.

ions and electrons randomly presented in the gap [2.2] begin to move under the high electric field, creating 'small' ionization events. If the electrode geometry produces locally high fields, such as at sharp edges, faint corona discharges may occur at the anode or cathode [52]. These pre-breakdown currents are usually very low (the current in Fig. 2.2). They serve to seed the gap with additional charge carriers while the electric field continues to build. Essentially, the pre-breakdown phase ends when the electric field becomes sufficient for a self-sustaining avalanche of electrons, i.e., when actual breakdown is imminent. The number of electrons and ions generated is sufficient to replace the lost, so the ionization avalanche can continue on its own. Once this condition is met, the spark discharge enters the breakdown phase.

2.1.2 Gas Breakdown

Breakdown is the abrupt formation of a highly conductive plasma channel across the gap. When a sufficiently high electric field is applied [2.3], free electrons in the gap rapidly accelerate toward the anode. These electrons collide with neutral gas molecules, ionizing them and creating new electrons and ions, creating an *electron avalanche* that grows exponentially [41]. This moment is so-called breakdown: a conductive channel bridges the gap. A surge of current on the order of hundreds of amperes [2.4] flows through the nascent plasma channel, albeit for an extremely short time (in the order of nanosecond) [53]. The voltage across the gap then collapses from the high breakdown value (Fig. 2.2). The end of breakdown is marked by the formation of a conductive plasma filament and the electrodes are heated up due to the intense energy flux, which seeds the next phase, the arc phase.

2.1.3 Arc Phase

In the arc phase (Phase (2) marked in Fig. 2.1), the spark discharge is maintained by a relatively high current following the breakdown. For a typical spark in SI-ICE, the arc phase current is in the order of hundreds *mA*. The heated cathode during the breakdown phase emits thermionic electrons and supply a large electron current [54]. As a results, the voltage needed to sustain the discharge is low.

[2.2] Mostly produced by the mother of nature.

[2.3] The breakdown voltage can be described by *Paschen's Law*, which is based on the *Townsend Breakdown Model*. It is deserved to be mentioned that this mechanism is inapplicable in high pressure, long gaps or considerable overvoltage conditions, like nanosecond pulsed discharges, where *Streamer Theory* becomes more suitable.

[2.4] It is not recorded in Fig. 2.1 and Fig. 2.2. Such high current was digitally filtered out during measurements because of its potential damage to the oscilloscope.

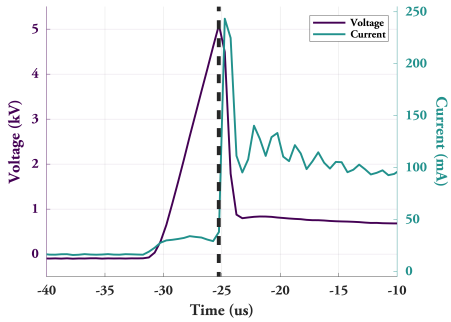

Figure 2.2: **The voltage and current waveform in the vicinity of gas breakdown.**
The dashed black line indicates the moment of breakdown, when the voltage reaches the highest value.

2.1.4 Glow Phase

As the stored electric energy is depleted, the spark discharge transitions into the glow phase (Phase (4) marked in Fig. 2.1). The spark discharge in glow phase is maintained at a lower current (typically $\lesssim$ 50 - 100 *mA*) compared with the value during arc phase. Opertaing with a 'cold' cathode, the primary mechanism sustaining the plasma becomes secondary electron emission from the cathode by photons or ions, rather than thermionic emission [54]. This process is far less efficient in terms of supplying electrons. Thus, the voltage drop near the cathode increases and becomes much higher to sustain the current. As a result, the spark voltage in Fig. 2.1 rises again, while the current remains decreasing.

2.1.5 Arc - Glow Transition

As the arc turns to the glow, a second voltage plateau in the voltage waveform is usually observed, which is shown in Fig. 2.3. However, the transition between arc and glow in a spark is not always a simple, single switch. The two modes can 'compete' during the spark events. In some sparks, multiple arc-glow-arc transitions occur as the current fluctuates [55, 56]. The exact sequence depends on factors like electrode material, gas pressure, and circuit inductance. While from a fundamental perspective, the key distinction is how the plasma gets its electrons. For arc, it's thermionic from hot cathode spots and for glow, the secondary emission becomes dominant. Generally, higher current or a readily heated cathode favor arc mode, whereas lower current or 'cold' cathodes favor glow mode.

2.1.6 AC Spark

Most conventional ignition systems produce a unidirectional spark (*DC spark*), meaning the current flows in only one direction across the gap. In such DC sparks, one electrode remains the cathode and the other the anode for the duration of the discharge (as Fig. 2.1). In contrast, an alternating-current discharge (*AC spark*) swaps the polarity of the electrodes

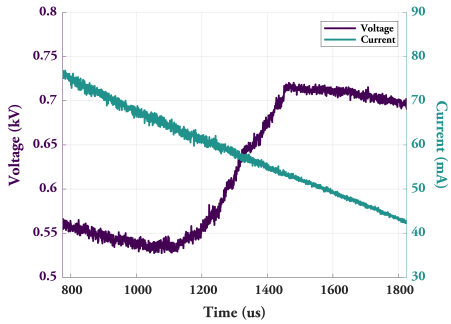

Figure 2.3: The voltage and current during arc-glow transition.

each half-cycle, resulting in a bidirectional spark. The voltage and current waveforms of a AC spark are presented in Fig. 2.4, which is produced by a newly developed capacitive ignition system used in this thesis.

At the beginning phase, a breakdown occurs when the voltage across the spark gap exceeds the threshold, causing the initiation of the spark. In the first following half-cycle, the AC spark behaves similar to a DC one, which persists until the current naturally falls to zero at the end. The plasma channel cannot be maintained and the spark momentarily extinguishes.

In the next half-cycle, the voltage builds up with opposite polarity and the spark re-ignites. Notably, from the right plot in Fig. 2.4, the voltage required is significantly lower than the breakdown voltage in the beginning phase. This is because residual ionized gas from the previous discharge remains in the gap [2.5], which facilitates the re-ignition and initiate the

[2.5] Similar to the phenomenon *plasma afterglow*.

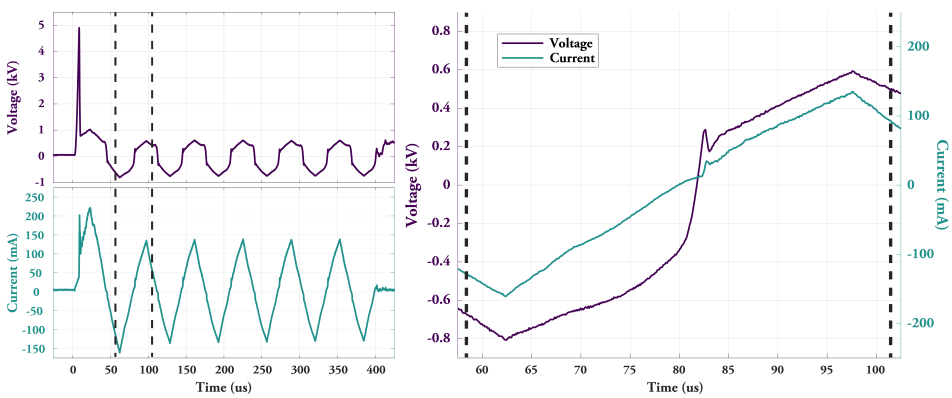

Figure 2.4: **Left:** The voltage and current characteristic waveform of the AC sparks used in this thesis, measured in atmospheric condition across a 1.2 mm gap. **Right:** The sudden increase in spark voltage at the moment of polarity reversal. The black dashed lines mark the intercepted half-cycle.

next half-cycle discharge. From the voltage and current behavior, it can be considered that each half-cycle of an AC spark behaves like a short DC spark. In other words, after each re-ignition, the AC discharge evolves through the same characteristic phases observed in DC discharges —namely, the arc phase, the glow phase, or their transitions —depending on the instantaneous voltage and current within the half-cycle.

2.2 Spark ignition

Ignition is the very first stage of combustion, which starts with a reactive mixture and evolves into a self-sustaining flame [57]. Ignition can occur spontaneously or be forced by an external energy source. Forced ignition means using an external energy source to initiate combustion. Various methods have been developed, such as electric spark, laser ignition, hot surface ignition, pilot flame, and even shock wave ignition. Among these, the electric spark is by far the most common in gasoline engines due to its reliability, simplicity, and precise timing control.

When a spark discharges, it deposits a certain amount of energy into a very small volume of the fuel-air mixture in the form of a plasma kernel. Highly reactive radicals (such as H, O, OH) are formed, which will kick-start the chain reactions of combustion [51]. A tiny kernel of burning gas is then formed. From that point, if conditions are favorable [2.6], the flame kernel will grow and a self-propagating flame front develops [58]. The spark's role is thus to reliably create a flame kernel above the minimum ignition energy and volume required for sustained combustion. Increasing the spark energy or using a longer-duration spark can enlarge the flame kernel and improve the chance of a successful ignition, especially under lean [2.7] or high-flow conditions [59]. However, more energy will also induce an increase in electrode wear (i.e., the subject of the thesis), so there is a trade-off.

2.2.1 Technical reality

The history of electric ignition system and spark plug [2.8] is as long as the internal combustion piston engine, which can be traced back to 19th century [28]. The whole system typically consists of an electric energy storage, a triggering switch, an extension and a spark plug. Despite the large number of different designs, both experimentally and commerically, the equivalent circuit can be simply described by Fig. 2.5 [2.9]. A coil (in the inductive system) or a capacitor (in the capacitive system) is used to store electrical energy and when triggered, a high-voltage pulse is delivered to the spark plug. The spark energy can be calculted by

[2.6] Several factors determine whether the spark ignition is successful: the amount of energy deposited, the duration over which it's deposited, the size of the initial plasma kernel, the local mixture composition and turbulence, and the quenching effects of the electrodes.

[2.7] Hydrogen is an excellent example, which normally run with super-lean to reduced NO_x formation.

[2.8] First commerically viable ignition system was invented by G. Honold from the company Robert Bosch.

[2.9] The figure is made based on Figure 1 in [51].

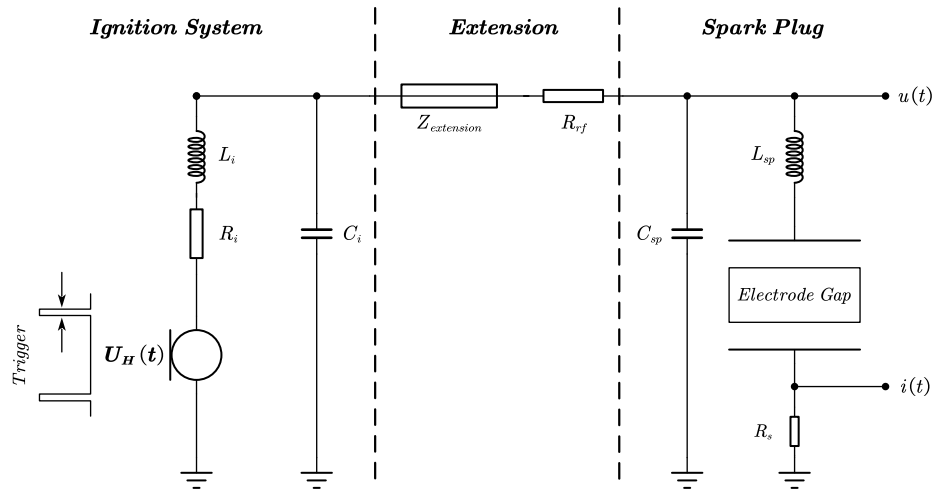

Figure 2.5: **Equivalent circuit of electric ignition sytems.**
Trigger: Signal from MCU, $U_H(t)$: High-voltage pulse, R_i: Coil resistance, L_i: Coil inductance, C_i: Coil capacity, $Z_{extension}$: Impedance of the extension, R_{rf}: Resistance of the extension for radio frequency oscillation damping, C_{sp}: Capacitance of the spark plug, L_{sp}: Inductance of the spark plug, $u(t)$: Voltage monitor, $i(t)$: Current monitor, R_s: Shunt resistance for current monitor.

integrating the product of the measured spark voltage $u(t)$ and current $i(t)$ over the entire discharge duration t with Eq. 2.1.

$$W_{spark} = \int_0^t u(t) \cdot i(t)\, dt. \tag{2.1}$$

Spark Plug

The spark plug itself is a deceptively simple but crucial device. A schematic drawing of a J-gap spark plug is presented in Fig. 2.6 [2.10]. The spark plug has a center electrode and a ground electrode. An insulator isolates the center electrode and allows the voltage to build until breakdown occurs in the gap between the two electrodes. It is designed such that the spark kernel protrudes into the combustion chamber for good access to the mixture, but at the same time the electrodes should not be so large as to quench the flame [60].

2.3 Spark-electrode interaction

Once the spark is formed, the plasma and the electrodes [2.11] are in close interactions. The electrically conducting plasma channel exchanges energy and particles with the electrode

[2.10] The figure is originally generated using an AI with the author's prompt.
[2.11] The electrdodes are mostly made of metal alloys to benifit the performance and the lifetime.

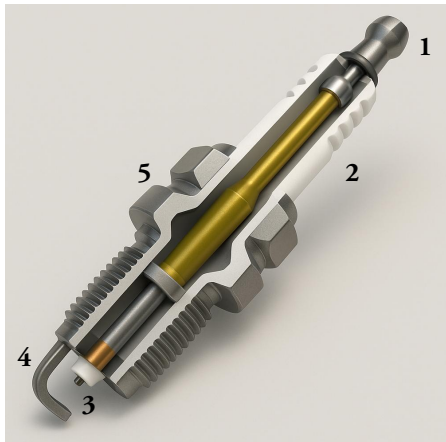

Figure 2.6: **Schematic drawing of spark plug with section view.**
1: Terminal, connected with the ignition system. 2: Insulation, the length of which can also be used to control the heat transfer of spark plug. 3: Central electrode, connected with the terminal through an internal core with high electrical conductivity. 4: Ground (or side) electrode, connected with the engine through thread. 5: Hex head.

surfaces. This plasma-material interaction governs how the electrodes wear out with repeated sparking. In this section, the fundamental interactions between the spark plasma and the electrodes are briefly discussed, focusing on the different roles of the cathode and anode in the discharge. Then, the current research status of electrode wear identified in literatures is overviewed.

Ion - cathode interaction

Positive ions from the plasma are accelerated toward the cathode by the electric field. These ions strike the cathode surface with significant kinetic energy. Ion bombardment is one of the most important processes at the cathode and delivers the ion energy to the surface [61].

For the arc, the ions are rapidly deposited in a very small area (the cathode spot), leading to intense local heating [62, 63]. If the ion current density at cathode spot is enormous, the molten pool will be formed and the evaporation will start if the energy is high enough. While for the glow, the cathode is relatively 'cool'. The cathode spots do not form and the current density is lower. However, the high voltage in glow due to the inefficiency of ion-induced electron emission makes the cathode subjected to a continuous rain of ions that gradually erodes the surface by knocking atoms out (i.e., sputtering) [64]. Such ion-cathode interaction is widely ultilized in material processing. For example, ion beam etching uses ions to sputter material from a target surface [61].

Electron - anode interaction

At the anode, the situation is opposite: electrons are accelerated toward the anode and hit its surface. An electron has less mass than an ion and thus travel much faster. Most of the electron's kinetic energy will be deposited as heat in the anode material [65]. If the current is high, this can cause considerable heating of the anode, potentially enough to locally melt it [66].

For example, in an electric arc furnace or arc welding, the anode develop 'anode spots' where intense electron flux creates hot spots that can vaporize metal [67]. There is also something known as 'explosive electron emission' at the anode in certain transient sparks [68]. Essentially, if the anode tip gets extremely hot, it can explosively emit vapor and electrons.

2.3.1 Mechanisms of electrode wear

Over the years, researchers have proposed several mechanisms to explain how electrical discharges erode electrode material theoretically and experimentally. The four most well-known mechanisms identified will be briefly discussed.

Sputtering refers to the process by which energetic particles (in the thesis, ions from the plasma) knock atoms out of the electrode surface [64, 69–71]. When a high-energy ion strikes the metal lattice, it transfers momentum to the target atoms. Through a series of collisions, some atoms near the surface may gain enough energy to overcome the binding energy and escape from the surface into the gas phase. The ejected atoms are typically neutral metal atoms that have been physically dislodged.

For bulk material, most sputtered atoms tend to eject back along the direction from which the ions came, which is called 'back-sputtering' [72]. In other words, ions from the plasma cause atoms to be ejected from the cathode surface back into the plasma. Based on the theroy developed by P. Sigmund [69], the primary backsputtering yield S_Y is mainly dependend on the ion's energy, the masses of the ion and target atoms, the incident angle, and the target material's binding energy. For spark discharge, the ions are mostly N_2^+, O_2^+, etc., from air. With energies ranging from tens to hundreds of eV, typical electrode metals (e.g. Ni, Pt, Ir) can be sputterred out.

Evaporation, on the other hand, is a thermal process: the plasma heats the electrode surface so much that the metal locally boils and vaporizes. The idea is that hot spots form tiny 'boiling craters'. The metal in the spots is heated to its boiling point (T_b) and continually vaporizes during the discharge. This mechanism was considered dominant by F.L. Jones [73–75]. The classic model proposed by him assumed that the energy input W_{spark} after a certain time t to the hot spots is balanced by the losses and the energy needed for evaporation E_v, which can be expressed as

$$E_v = W_{spark} - rt - qt - Z. \tag{2.2}$$

r is the radiation rate from the hot spots to the environment with a temperature T based on *Stefan-Boltzmann Law*, which is

$$r = \varepsilon\sigma S(T_b^4 - T^4). \tag{2.3}$$

q is the loss rate of energy by heat conduction, which can be estimated by

$$q = 2k\sqrt{\pi S}(T_b - T). \tag{2.4}$$

Z stands for all other losses, such as the heat convection and conduction with the crossflow between the electrodes, which can be considered negligible compared to r and q.

In the model, assuming a fixed heat flux on the electrode surface, the temperature rise T_t after the certain time t can be estimated using a 1D heat conduction equation [2.12], which equals

$$T_t = 2\sqrt{t}\frac{P}{S}\frac{1}{\sqrt{\pi kc\varrho}}. \tag{2.5}$$

If the temperature T_t reach the boiling temperature of the electrodes T_b, the energy E_v needed to evaporate certain mass of electrode material can then be calculated as

$$E_v = mc_s(T_m - T) + m\Delta H_{fus} + mc_l(T_b - T_m) + m\Delta H_{vap}. \tag{2.6}$$

Based on this, the properties that matter most for an electrode material are its boiling point and thermal conductivity. A material with high boiling point and excellent thermal conductivity will resist forming a boiling spot. It will conduct the heat away and require more energy to vaporize the material. For example, tungsten and iridium have extremely high boiling points, and indeed they are found to have lower erosion rates compared to copper or nickel [33]. However, this model not only neglects the chemical reactions, but also can not explain certain features, such as the discrete molten craters and droplets found on electrodes. Another mechanism is thus proposed, particle ejection.

Particle/droplet ejection is provided by E.W. Gray and colleagues in the 1970s involving molten metal being physically expelled from the electrode [76–78]. During the discharge,

[2.12] $\frac{\partial T(x,t)}{\partial t} = a\frac{\partial^2 T(x,t)}{\partial x^2}$ $(x \geq 0, t > 0)$, with a constant heat flux $-k\left.\frac{\partial T(x,t)}{\partial x}\right|_{x=0} = \frac{P}{S}$ (for $t > 0$).

a small molten pool forms at the cathode spot. The incoming positive ion stream exerts a pressure on this molten pool, effectively pushing the liquid metal outward toward the edges of the crater. This creates a hydrodynamic pressure gradient in the molten metal, generating a recoil force. As the discharge ends, the ion bombardment stops instantaneously. The force that was pushing outward (ion pressure) vanishes, but the molten metal that was set in motion continues due to inertia. The recoil drives the liquid metal inward and upward since the confining pressure is gone. The result is that the molten metal can pinch off into one or more droplets. What remains on the electrode is a crater and often a rim or splattered edge where some molten metal was pushed outward.

Researchers also observed similar features on spark plug electrodes: craters often with a distinctive 'lip' and tiny droplets of electrode material scattered around [40, 79]. This strongly supports the particle ejection mechanism as one of the major erosion processes in spark discharges.

Oxide removal is more chemical in nature: erosion due to the formation and subsequent removal of oxide layers on the electrode, rather than direct metal removal. The basic idea is that the presence of oxygen leads to oxidation of the hot electrode surfaces during spark. Metals can form oxide compounds when heated under activated oxygen. These oxide layers may be brittle or have different density from the metal, and they can flake off or spall due to thermal stresses. If each spark forms a bit of oxide which later cracks or is blown off, the metal underneath is gradually consumed in the process. In other words, the spark doesn't directly gouge out metal; instead it facilitates oxidation and then the oxide breaks away and takes material with it. This gives a better explanation why high-melting metals still wear.

Y. Shimanokami supported this model by showing that using materials with high melting points and excellent oxidation resistance improved spark plug life [31]. Such materials, like iridium, exhibited significantly lower wear in long-term engine tests. J. Rager and colleagues performed spark erosion tests in controlled atmospheres [80, 81]. They found that in pure nitrogen, the electrode erosion was almost negligible. But in air, the same electrodes showed substantial erosion.

This mechanism suggest that without oxygen, the three abovementioned wear processes were not sufficient to cause major loss. However, since spark plugs are designed for ignition in ICEs where oxygen is inherently present, this mechanism is regarded more as an added effect than a primary consideration in the following content.

Remark

Approaching the end of this chapter, it is clear that spark discharge is a multi-phase phenomenon with complex plasma-material interactions. It can be imagined that in reality, the discussed mechanisms are not mutually exclusive. All can occur in one single spark, breakdown may cause sputtering, arc may cause evaporation and material ejection, and

glow may cause sputtering. All the previously mentioned studies and proposed mechanisms are undoubtedly valuable, while they primarily rely on long-term endurance tests or isolated single-spark experiments. Such *ex-situ* measurements cannot transfer *'may'* to *'be'*. Thus, the main work of this thesis is tyring to fill this gap as a pioneer. With the *in-situ* laser-based optical diagnostic methods, it is possible to identify how each phase of the spark contributes to the electrode wear.

Chapter III

Towards *in-situ*

If I have seen a little further,
it is by standing on the shoulders of giants.

— Isaac Newton

Now the questions are raised: can we visualize the material 'leaving' electrode that leads to spark plug wear during spark discharge, and if so, how? So, the journey of lased-based optical diagnostics starts from this chapter. The fundament of atomic physics is briefly introduced as a foundation. *Optical Emission Spectroscopy* for passive emission monitoring and *Laser-induced Fluorescence* for active and sensitive detection are then delved into. The aim is to provide a comprehensive understanding of how element's spectral 'fingerprint' arises and how these fingerprints can be used for the diagnostics of electrode wear from an application perspective.

3.1 Fundament of atomic physics

Understanding atomic spectra starts with understanding the structure of the atom and how electrons are arranged in discrete energy levels. Atoms are not mini solar systems with electrons free to orbit at any radius; instead, they have quantized energy states [82], which is simply illustrated by a nickel atom in Fig. 3.1. The unique spectral lines of each element originate from electrons transitioning between these specific energy levels.

Term Symbol

Four quantum numbers (n, ℓ, m_ℓ, m_s) are used to uniquely identify the state of an electron in an atom. The arrangement of different electrons is described using an electron configuration notation, which lists the occupied subshells and the number of electrons in each. However, an electron configuration alone does not uniquely specify the quantum state of a multi-electron atom when subshells are partially filled [83]. For example, if two electrons occupy the same subshell (like the two 2p electrons in carbon), there are multiple ways to arrange their individual m_ℓ and m_s values. As a result, the total angular momentum states for the atom are different, which have slightly different energies due to electron-electron interactions and spin coupling. They manifest as multiple spectral lines even for the same configuration. To distinguish these difference, the term symbol and the total angular momentum quantum numbers J are used.

There are two mainly used shemes for multi-electron atoms, LS (Russell-Saunders) coupling and jj coupling, which differ in how total angular momentum J is built and how atomic energy levels ('term symbols') are labeled [83]. Both have limitations, depending on the relative strength of electrostatic interactions versus spin-orbit coupling. For lighter atoms, LS coupling is a good approximation, where spin-orbit interaction is weak compared to

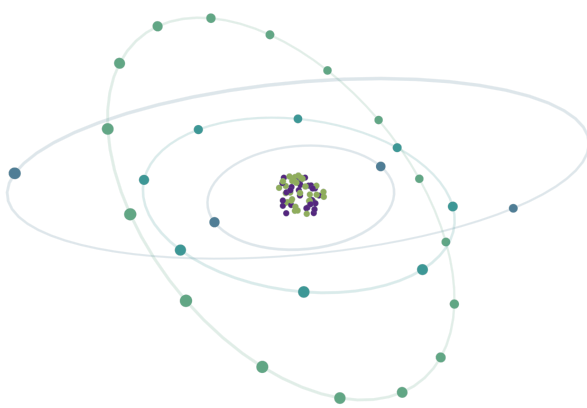

Figure 3.1: Simplified illustration of nickel, with the atomic number 28.

electron-electron repulsion. For heavier atoms, *jj* coupling becomes appropriate as spin-orbit effects becomes strong.

These two limiting models delineate how total *J* is constructed and how terms are labeled. Understanding both schemes and their domains of validity is essential for interpreting atomic spectra. However, it is important to remember that real atoms often lie between these extremes, requiring intermediate coupling treatments, for example, *JL* coupling for some nickel energy levels [84].

3.2 Optical emission spectroscopy

OES is a foundational technique in spectroscopy where one analyzes the light emitted by excited species to determine what elements (and sometimes what quantities of those elements) are present in the probe volume. The basic principle is straightforward: if a substance is heated, electrically excited, or otherwise energized, its constituent atoms will emit light at specific wavelengths as their electrons transfer to lower energy levels. By measuring the spectrum of the emission and identifying the wavelengths (or frequencies) present, one can infer which atoms produced them, because each element has a unique set of allowed transitions. In the context of spark plug wear, OES allows us to directly see and identify the materials in gas phase (such as nickel) that stemmed from the electrodes.

3.2.1 Selection Rules

Before going deep to OES, the selection rules for atomic electronic transitions is need to be briefly introduced. Atoms have discrete energy levels as discussed, and a transition between two energy levels occurs when an electron moves from one level to another. The set of all possible transitions between atom's energy levels gives rise to that element's spectrum. However, not all imaginable transitions actually occur. Certain selection rules must be obeyed based on fundamental conservation laws (such as conservation of angular momentum) and the quantum mechanical properties of the states [85]. Selection rules determine whether a transition between two quantum states is allowed (i.e., has a high probability and hence an observable spectral line) or forbidden (i.e., highly unlikely, resulting in either no line or a very weak line). Therefore, when analyzing spectra for diagnostic purposes (like identifying elements from their lines), we are usually dealing with the allowed lines that obey the above selection rules.

3.2.2 Broadening Effect

Spectral lines are never perfectly sharp single wavelengths, but instead appear broadened due to various physical mechanisms. For example, the observed nickel lines in Fig. 3.2 are clearly broadened instead of infinitesimally narrow. Multiple factors cause emission lines

to have a finite width (i.e. line broadening) rather than delta functions. Key broadening effects include natural broadening, Doppler broadening, and pressure broadening [82]. In addition, instrumental resolution can also broaden observed lines by a certain width.

Natural broadening (also called lifetime broadening) is an intrinsic effect arising from the finite lifetime of excited atomic states.
Doppler broadening is caused by the thermal motion of emitting atoms, which have a Maxwell-Boltzmann distribution of velocities in random directions. As a result, the emission from many atoms produces a spread of Doppler-shifted frequencies around the central frequency.
Pressure broadening (also known as collisional broadening) occurs when interactions between the emitting atom and other particles perturb the emission process. Frequent collisions cause slight random shifts in the energy levels, producing an uncertainty in the emitted frequency and thus broadening the line.
Stark broadening results from that the electric fields of nearby ions and electrons cause splitting and broadening of energy levels (the Stark effect), spreading the emitted line over a range of wavelengths.

Actually, the line shape and width result from a convolution of different broadening mechanisms. The resulting profile is often a Voigt shape, which is a convolution of a Lorentzian function with a Gaussian function.

3.2.3 Application

Typically, a spectrometer [3.1] is used to disperse the detected signal into its component wavelengths and recorded by the attached detector [3.2] as an emission spectrum (intensity vs wavelength). Each peak in the spectrum corresponds to a particular transition in a specific element and the recorded signal can be expressed by Eq. 3.1. R_λ is the optical reponse of the spectrometer, which is wavelength-dependent. $n_{excited}$ is the population of the excited state and $A_{excited}$ is the Einstein spontaneous emission coefficient.

$$I_\lambda = R_\lambda \cdot n_{excited} \cdot A_{excited}. \tag{3.1}$$

OES is widely applied in the field of material science, particularly for elemental analysis [86–89]. For example, in analytical chemistry, ICP-OES are standard for detecting trace amount of elements. In our case of spark plug wear diagnostics, OES offers a quick way to detect the metals or other elements that are presenting in the spark gap. A spark plug

[3.1] For spectrometer, F number, slit width and grating density are important for achieving optimal spectral resolution and signal intensity. After calibration, the exact location of the wavelength and the corresponding spectral response can be known.

[3.2] Noramlly, the detector is a 1D/2D CCD or CMOS array.

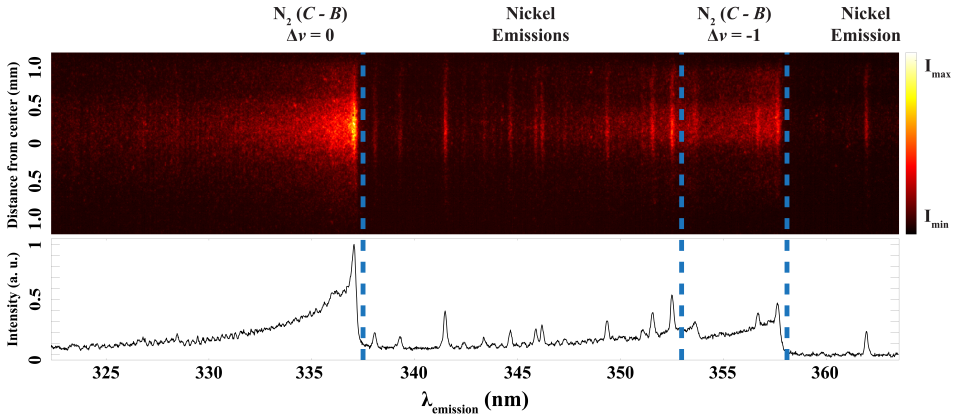

Figure 3.2: **Plasma emission and detected nickel emission in the wavelength range from 323 nm to 363 nm.** Transitions of detected emissions are listed in Table II of **Paper I**.

typically has electrodes made of nickel alloy or noble metals, like iridium or platinum. These metal atoms have many possible lines, which often in the visible and ultraviolet ranges.

Limitations

OES generally requires a reasonably high population of atoms in excited states to get a detectable signal. If the erosion is extremely slight, the metal atom density might be low and their emission is very weak. If the intensity is at the level as same as the noise, the target species is unable to be distinguished.

Spectral interferences is another issue. If multiple elements have lines in the same spectral region, a low-resolution spectrometer might confuse them. In practice, spectrometer with a relatively high resolution or well-known line positions could mitigate this.

OES signals are inherently line-of-sight integrated, meaning that the detected spectrum represents the cumulative emission along the entire optical path. In a complex environment, observing through an optical window may result in a spectrum that includes both the desired emission from the target species and unwanted background radiation. To improve the SNR, time-gating [3.3] or spectral gating [3.4] can be employed.

Nevertheless, OES remains a powerful and relatively simple tool to monitor atomic species. In the case of spark plug wear, a general idea whether the atoms eroded from the electrode exist or not is gained during spark discharges. Considering OES cannot detect ground-state atoms that never get excited, a more powerful laser diagnostics tool, LIF, is thus ultilized.

[3.3] The detector can be gated to exclude intense background, if the signal has a relative long lifetime.

[3.4] For example, in Fig. 3.2, one can focus on the nickel emission lines located between two intense nitrogen emission bands ($C^3\Pi_u \rightarrow B^3\Pi_g, \Delta v = -1, 0$).

3.3 Laser-induced fluorescence

While OES relies on passive emission, LIF is an active spectroscopic technique. The basic principle is illustrated in Fig. 3.3 [3.5] and more detailed description can be seen in [90]. The atoms or molecules of interest are excited using a laser with a specific wavelength, and the subsequent spontaneous fluorescence is captured by certain detectors. LIF is renowned for its high sensitivity and selectivity, which can detect even trace species that would be difficult to see with OES. Also, excellent spatial and temporal resolution can be achieved by focusing the laser with short pulse duration to a small region. In the context of electrode wear, LIF can be employed to detect ground-state metal atoms in gas phase, such as nickel within the spark plug gap.

3.3.1 Setup

A typical experimental setup for LIF is given in Fig. 3.4, a laser beam is tuned to a wavelength that corresponds to a transition of the target species. When the laser is fired, photons are absorbed by the atoms, elevating electrons from a lower state [3.6] to an excited state. Shortly after, those excited atoms will spontaneously emit photons as they decay back down, which

[3.5] For photoionization ($M + h\nu \rightarrow M^+ + e^-$), the excitation mostly needed below Far-UV region (< 200 nm). Predissociation ($AB + h\nu \rightarrow A + B$) exists in molecules.

[3.6] The lower state is often the ground state due to Boltzmann distribution.

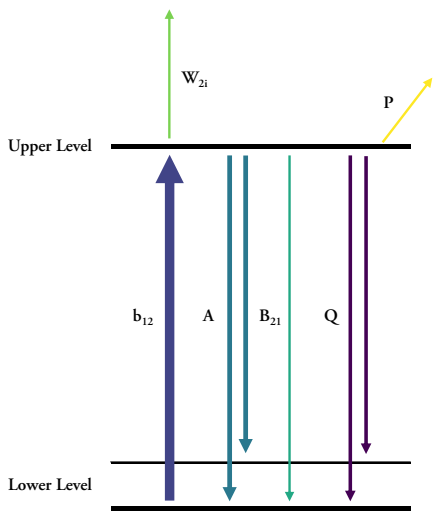

Figure 3.3: **Simplified energy level diagram for LIF modelling.**
b_{12}: Absorption of excitation photon, A: Spontaneous emission, B_{21}: Stimulated emission, Q: Non-radiative de-excitation by collisional quenching, W_{2i}: Photoionization, P: Predissociation.

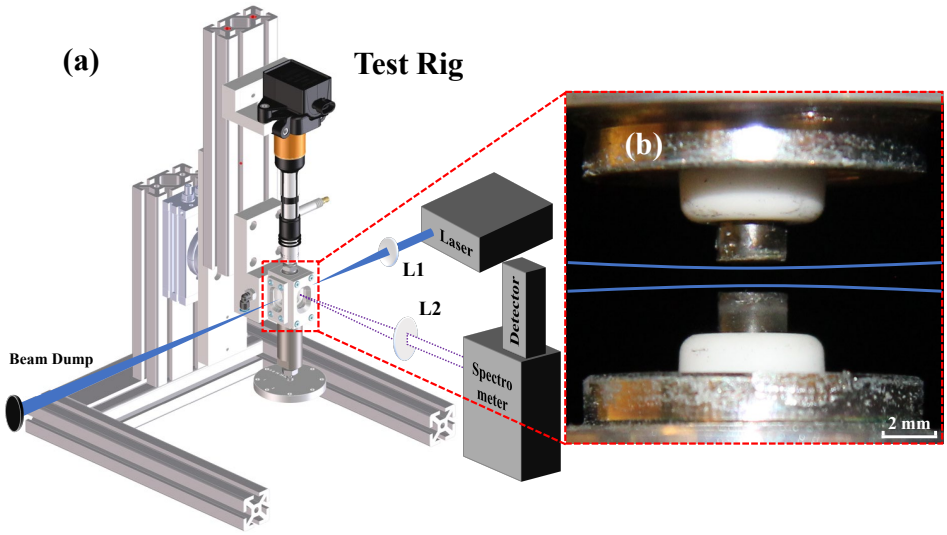

Figure 3.4: **The typical experimental configuration of LIF, also used in the thesis work.**
(a) Schematic illustration. (b) A close look at the probe volume. The blue lines indicate the Gaussian laser beam. L_1: Focusing lens, sphrical for point measurements and cylinderical for two-dimensional planar measurements. L_2: Signal collecting lens.

is so-called fluorescence. By detecting and collecting the fluorescence signal [3.7], one can infer the presence and quantity of the target species.

Detectors

The fluorescence photons are collected [3.8] by different detectors, oftenly intensified cameras or photomultiplier tubes. A spectrometer can be used together if spectral resolution is needed, like the setup in Fig. 3.4.

Intensified camera is a time-resolved imaging device that couples a CCD or CMOS sensor with a MCP image intensifier for ultralow-light detection. Incoming photons strike a photocathode at the front of the intensifier, releasing photoelectrons that are multiplied by the MCP, which is a thin disc of densely packed glass channels under high voltage. This electron cascade yields gains and can even enable single-photon sensitivity. The amplified electrons then strikes a phosphor screen [3.9], converting back to an optical image that is relayed to the sensor. The MCP can be electronically gated on and off within nanoseconds intervals, which provides a precise temporal resolution and enables rejection of background

[3.7] From the theroy discussed before, the fluorescence can be at either the same wavelength as the laser or at a different wavelength if the excited state decays to some other energy level. In practical, the later one is preferred to remove the background of the excitation laser.

[3.8] Typically at 90 degrees perpendicular to the incident beam.

[3.9] Various phosphors are designed for different purposes. For example, if one want a fast reponse, phosphor with a short lifetime is preferable.

light outside the gate window.

Photomultiplier tube is ultra-sensitive light detector widely used to capture weak fluorescence signals. A PMT consists of a vacuum tube with a photosensitive cathode and a series of dynodes held at successively higher potentials. When a fluoresced photon from the probe strikes the cathode, it releases an electron via the photoelectric effect. This electron is electrostatically accelerated into the first dynode, knocking out multiple secondary electrons, which are in turn accelerated to the next dynode. Through multiple dynode stages, the single photoelectron is multiplied into a large electron pulse, which is collected at the anode as a measurable current or pulse. This internal amplification gives PMTs single-photon detection capability and excellent signal-to-noise characteristics. Moreover, PMT have a relative fast rise time. In LIF setups, PMT is typically synchronized with the pulsed laser excitation, which enables the detection of fluorescence decay profiles following the excitation pulse.

Tunable laser systems

In 1917, Einstein proposed that in the interaction between the radiation field and matter, the molecules or atoms can generate stimulated emission or absorption of photons under the excitation of light. This has been implied that light amplification by stimulated emission of radiation (LASER) can be achieved if the number of electrons is reversed according to Boltzmann distribution. Years later, the first laser was born in 1960 by T. Maiman, which works with the medium - Ruby [91].

Since the advent of the laser, various types of lasers have emerged, from gas lasers, semiconductors lasers to fiber lasers. Specifically, performing LIF requires an intense and short-pulsed light source to allow time-resolved measurements and high peak power. To locate the target transitions for nickel, a laser with tunable wavelengths and a narrow linewidth is also desired to specifically excite a particular transition without off-resonant excitation. The two tunable laser systems used in this theis were a picosecond laser system based on an OPG pumped by a fiber laser [3.10] and a conventional Nd:YAG pumped dye laser system [3.11]. With those two laser systems, not only LIF can be performed but also two other critical pieces of information for analyzing the fluorescence signal can be obtained.

Excitation spectrum by varying laser wavelength to find resonance peaks and measure absorption line profiles using dye laser with a narrower bandwidth.

[3.10] The OPG combines an OPO with a multi-pass OPA to generate widely tunable pulses, which is pumped by a high-power picosecond fiber laser. The OPO stage seeds the OPA, and a double-pass amplification scheme is used to boost pulse energy while maintaining beam quality. A spectral cleaning unit is incorporated as a filtering module to ensure a narrow bandwidth output.

[3.11] The Nd:YAG-pumped dye laser uses organic dye solutions as the gain medium. In this thesis, a Q-switched Nd:YAG laser with nanosecond pulses at 532 nm was used to illuminate dye cells, containing a mixture of DCM and LDS 698 solutions. The dye molecules fluoresce and, within a resonant cavity (mainly a diffraction grating as the wavelength-selective element), undergo stimulated emission to produce laser pulses. By selecting different dyes or tuning the grating in the cavity, the dye laser output can be tuned across a certain range.

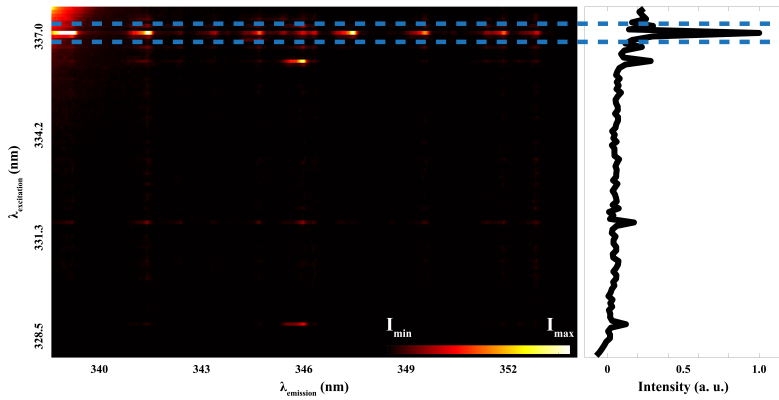

Figure 3.5: **Laser-induced fluorescence signal from nickel excited by the laser from 327.8 nm to 337.7 nm and detected in the range 338 nm to 353 nm.**
Respective transitions are listed in Table 1 of **Paper I**.

Fluorescence lifetime by observing the decay of the signal after the excitation laser pulse.

3.3.2 Excitation spectrum

For the interest in electrode wear, LIF would specifically target the metal atoms, like Ni, within the spark plug gap. The laser would be directed into the spark gap area at a controlled timing relative to the ignition spark. By scanning the laser wavelength across the nickel resonance and measuring the resulting fluorescence between the intense nitrogen emission bands (as shown in the OES result in Fig. 3.2), the optimal excitation transition can be identified to maximize signal detection and the SNR can thus be improved.

An excitation plot of nickel can be seen in Fig. 3.5, which was performed in a range of 10 nm from 327.8 nm to 337.7 nm, with a 0.1 nm step-size. The abscissa is the emission and the ordinate is the excitation. It can seen that the most robust fluorescence signals were observed when the excitation occurred at a wavelength of 337.0 nm. From the detailed transitions listed in Table I of **Paper I**, this transition is probed around 336.96 nm and the involved ground state of nickel, the most populated state, gives the explanation.

Fig. 3.5(*b*) is the corresponding normalized spectrum, which is integrated by the emission signals detected at each excitation wavelength. Several other possible excitation transitions were discerned in addition to the prominent peak at 337.0 nm. With the excitation spectrum, not only is the optimal excitation transition identified, but also the detected fluorescence signal stemming from target species is confirmed.

3.3.3 Fluorescence lifetime

When an atom is excited by the laser in LIF, there is a characteristic delay of the following emission, which is statistically described by the fluorescence lifetime of that excited state. The fluorescence lifetime, usually denoted τ, is the average time an atom stays in the excited state before emitting a photon and returning to a lower state. This is an intrinsic property of the atomic energy level, determined by the probabilities (Einstein A coefficiens) of allowed transitions from that level. For a level that can decay to lower levels i with transition probabilities A_{ji} (s^{-1}), the natural radiative lifetime is

$$\tau_0 = \frac{1}{\sum_i A_{ji}}. \tag{3.2}$$

The concept of fluorescence lifetime is important for LIF signals [92]. The number of photons emitted (and hence the signal) from an excited population is proportional to the fraction of excited atoms that actually emit before other processes deplete them. If an excited state has a long radiative lifetime, an excited atom could emit one photon given enough time - but if something else de-excites the atom first, the photon is quenched. In a dense environment, collisions can de-excite the atom non-radiatively, which is so-called collisional quenching. The effective lifetime in such a case is shorter than the natural radiative lifetime. Illustrated in Fig. 3.6, the detected fluorescence signal I_{LIF} from a single short-pulse excitation is:

$$I_{LIF} = \eta \int_{t_1}^{t_2} I_0 e^{-\frac{t}{\tau_0}}\, dt. \tag{3.3}$$

η is the constant combining the fluorescence collection efficiency and quantum yield of the detector. I_0 represents the peak fluorescence intensity. t_1 and t_2 give the opening and closing time of the gate function. If collisions add an extra decay path, the total decay rate increases and weakens the signal.

Collisional quenching

Without a vacuum-like environment, the presence of other species can easily shorten the fluorescence lifetime. These particles can collide with the excited atom and cause it to drop to a lower state without emitting a photon [3.12] [93]. The higher the pressure or particle density, the more likely quenching collisions become. The effective lifetime τ_{eff} in the presence of quenchers is given by:

[3.12] The energy normally turns into kinetic energy of the colliding partner or exciting that partner.

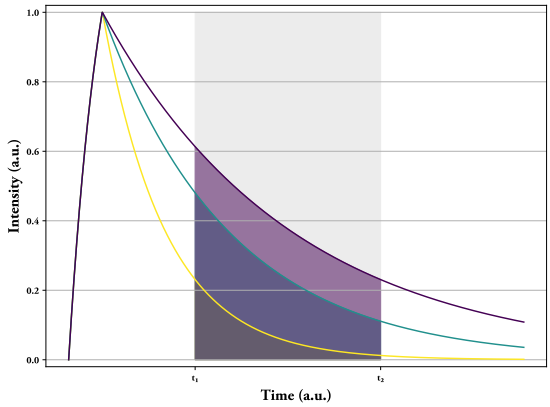

Figure 3.6: **Illustration of detected LIF signal with different fluorescence lifetimes.**
The grey zone shows the period of data collection. t_1 and t_2 indicate the opening and closing of the gate function.

$$\frac{1}{\tau_{\text{eff}}} = \frac{1}{\tau_0} + \sum_k q_k n_k \tag{3.4}$$

, where n_k is the number density of quencher species k and q_k is the quenching rate coefficient.

In the context of spark plug wear study, the fluorescence lifetime of the nickel transitions needs to be considered. Operating at a complex plasma enviroment, a relative high density of gas and possible impact from electrons and ions will induce a strong quenching effect. To correlate the intensity of measured LIF signal to the number density of nickel atoms from electrodes, the knowledge of effective fluorescence lifetime and how it changes across the duration of the spark discharge is necessarily needed.

Fig. 3.7 gives the effective fluorescence lifetime of nickel atoms produced by 3 ms DC sparks. The decay profile was capture by a PMT, which excited by a 337.0 nm picosecond laser. From the initiation of the discharge to the end, the measured lifetime stay constant at about 1.1 ns. As a comparsion, in vacuum and absence of other perturbations, the same excited energy level of nickel atoms has a lifetime in the order of tens of nanoseconds [94–97].

In summary, fluorescence lifetime is a one of the key parameters in LIF, which affects the intensity of the fluorescence signal and can be ultilized to optimize the detection. Also, the fluorescence decay can itself provide diagnostic information about the environment [98], like temperature and ambient pressure.

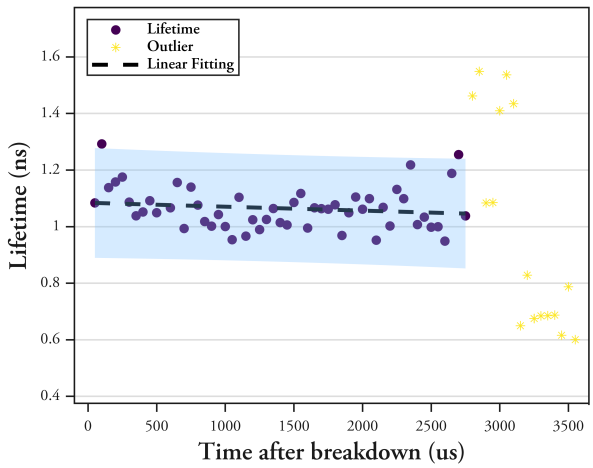

Figure 3.7: **Effective fluorescence lifetime of nickel atom during spark discharges in atmospheric pressure.** The shaded zone indicates the 95% confidence prediction bounds of the linear fitting.

3.3.4 Excitation intensity

For LIF, the relationship between the laser excitation intensity and the fluorescence signal can operate in two regimes: linear LIF and saturated LIF, which can be seen in 3.8.

At low excitation energies (i.e. weak laser intensity), the LIF process is in the linear regime. The fluorescence signal is directly proportional to the laser irradiance. However, the signal is sensitive to the quenching rate, resulting in difficult quantitative measurements in this

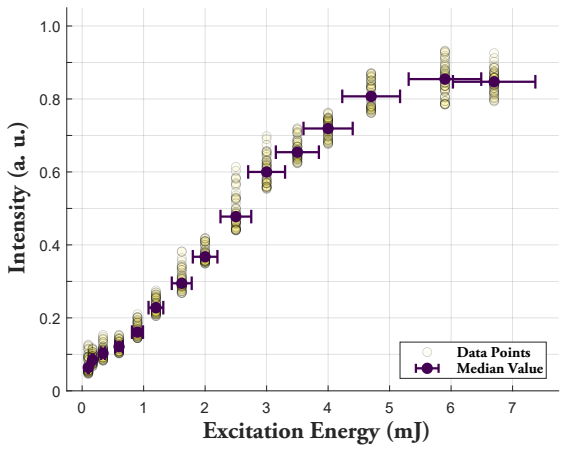

Figure 3.8: **The dependency of the intensity of laser-induced nickle fluoscence with excitation laser energy.** The laser works at the optimal excitation transition 336.96 nm.

regime.

At sufficiently high laser pulse energy or intensity, the LIF signal begins to deviate from linearity and saturate. In the saturated regime, the laser intensity is so strong that the absorption/excitation rate outpaces all depopulation processes, causing the excited-state population to approach its maximum. Essentially, the laser-driven transitions dominate over spontaneous decay and collisional de-excitation. Under complete saturation, the fluorescence signal is only dependent on the species population and is independent of both the laser power and the quenching rate. This is a key advantage of operating in the saturated regime: once achieved, the measurement is no longer sensitive to shot-to-shot laser fluctuations and collisional quenching effects in the probe medium. The signal is essentially at its theoretical maximum for the given number of fluorescing species.

Despite its benefits, achieving fully saturated LIF in practice can be challenging. It requires very high laser energies, and even then the laser beam often has a spatial intensity profile (e.g. Gaussian) such that only the central region is truly saturated while the edges remain in the linear regime. In other words, maintaining uniform saturation over the entire probe volume is difficult. Thus, in this thesis, the LIF measurements are working in the linear regime to ascertain a linear response.

Chapter IV

Key findings

Experimental physics is not only about knowledge and intuition,
but also about craftsmanship.

— Chao-Yang Zhang

Based on the necessary initial spectral study in Chapter III, two-dimensional LIF measurements were performed and some key findings will be discussed in this chapter. Two different mechanisms causing electrode wear are visualized for the first time within the spark plug gap. The evaporation model is refined based on the findings.

Ambient gas pressure was found to strongly influence detected laser-induced nickel fluorescence signal. At higher pressures, the LIF imaging revealed a more intense nickel vapor plume emanating from the electrode. At lower ambient pressures, by contrast, the nickel atoms is found concentrated close to the cathode surface, with certain expansion into the gap. These observations indicate that a lower-pressure environment promotes sputtering-driven erosion, whereas a higher-pressure environment results in a evaporation process, which is shown in Fig. 4.1.

4.1 Sputtering

Throughout all test conditions, sputtering is found to be one of the two primary erosion mechanisms for the nickel electrode. As discussed in Section 2.3, sputtering refers to the ejection of atoms from a solid surface due to the impact of energetic particles, typically ions, with sufficient kinetic energy. This mechanism is clearly evidenced in the time-resolved LIF images shown in Fig. 4.2. In these images, which span from 10 μs to 1750 μs after the initiation of the DC sparks, the sputtered nickel atoms are clearly visualized. The color scale on the right corresponds to relative emission intensity.

Sputtering becomes evident shortly after the breakdown phase of the discharge, particularly from around $T = 50$ μs onward. The bright spot on the cathode is the laser reflection from the metal surface, which can not be totally filtered out. This localized plume expands and intensifies through $T = 75$ μs to $T = 200$ μs, peaking in visibility around $T = 300$ μs. The persistence of emission even at later times ($T > 500$ μs) suggests sustained nickel atoms release, though with a decreasing intensity.

During the discharge, the cathode accelerates positive ions, toward the electrode surface. These ions can possess energies in the range of tens to hundreds of eV [4.1]. Upon impacting the cathode surface, these ions transfer momentum to nickel atoms. If the transferred energy exceeds the surface binding energy, individual nickel atoms are ejected from the lattice into the gas phase, i.e. into the spark plug gap. The evolution of the fluorescence

[4.1] Estimated with the value of voltage (~ 1000 V) in Fig. 2.1 and a 1 mm gap.

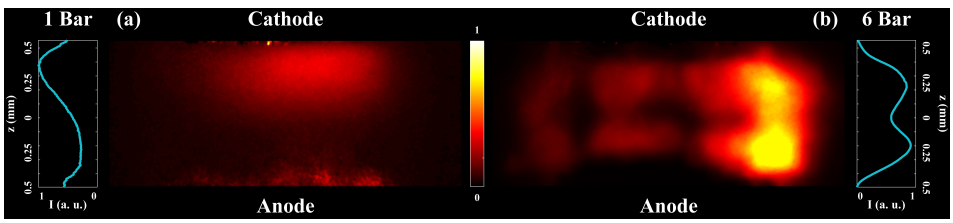

Figure 4.1: **Laser-induced fluorescence images of nickel, obtained by averaging 100 spark events at the time of peak signal under different ambient pressures.**
(a) Captured at 350 µs after breakdown at 1 bar and (b) captured at 20 µs after breakdown at 6 bar.

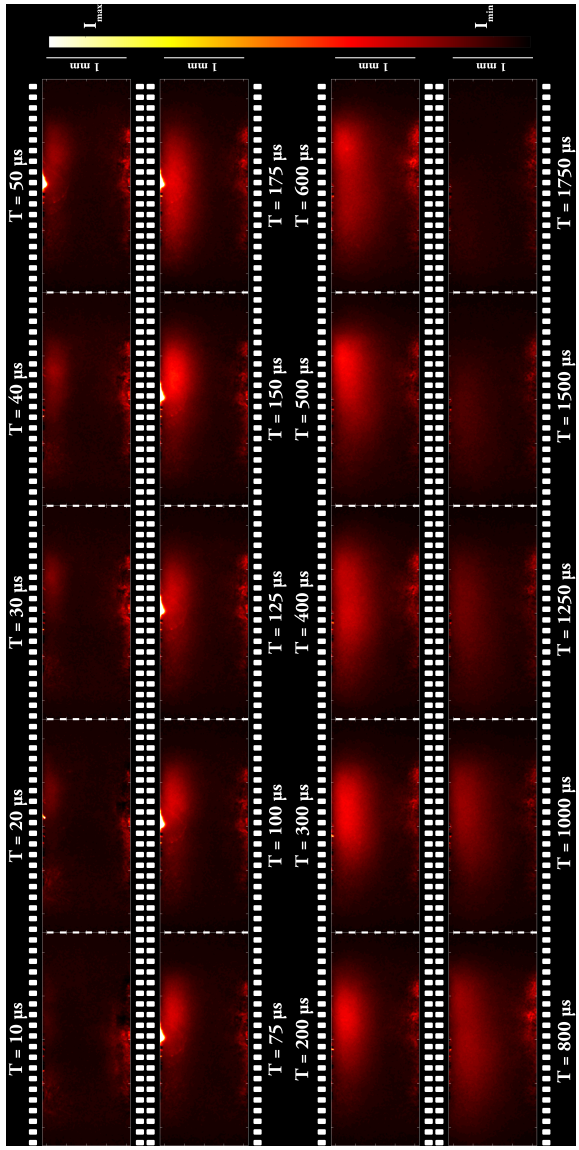

Figure 4.2: **Time-resolved laser-induced fluorescence images of nickel at 1 bar ambient pressure.**
Each frame represents the average of 100 spark events and corresponds to a specific delay time after the breakdown phase during a 3 ms DC spark discharge. The images show the distribution of nickel atoms within the 1 mm electrode gap of the spark plug. The cathode is located at the top, and the anode at the bottom.

pattern in Fig. 4.2 provides the visual evidence of the ion-induced sputtering.

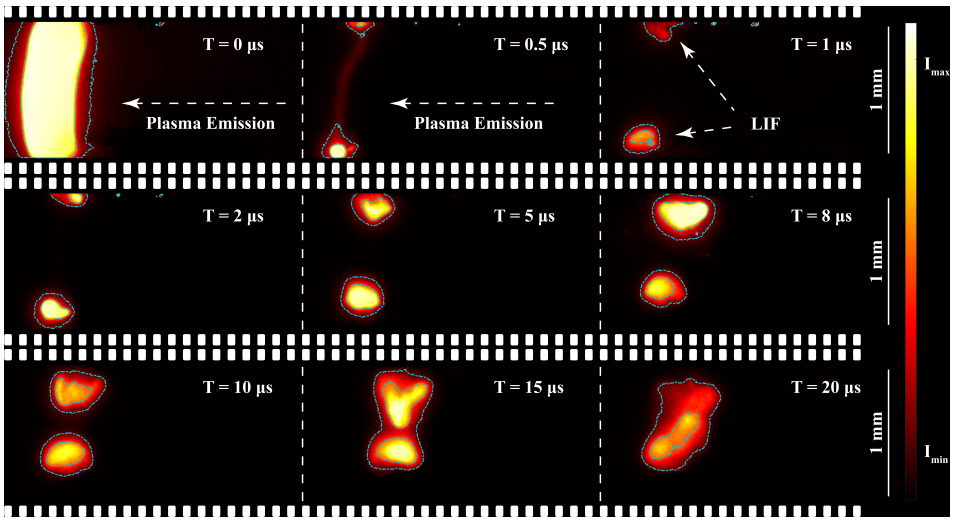

Figure 4.3: **Single shot laser-induced fluorescence images of nickel at 6 bar ambient pressure, captured from pre-breakdown phase to 20 μs after.**
Blue dashed contours indicate isolines of equal LIF intensity.

4.2 Evaporation

Evaporation was confirmed as the dominant erosion mechanism of the nickel electrode under elevated ambient pressure conditions. The early phase of the evaporation process is shown in Fig. 4.3. The electrode surface is rapidly heated to a high temperature and once the local temperature approaches or exceeds the boiling point, surface atoms acquire sufficient thermal energy to transition into the gas phase, initiating evaporation. This process results in the formation of a nickel vapor cloud above the electrode surface, particularly at localized hot spots.

The evolution of the evaporated vapor afterwards is presented by a time-resolved LIF image series of neutral nickel atoms in Fig. 4.4. The image sequence gives the spatial and temporal evolution of the Ni vapor cloud from 10 μs to 1750 μs after the spark initiation. Each frame corresponds to a distinct time delay after the breakdown.

From 10 μs to 50 μs, intense LIF signals are observed, particularly around $T = 10$ μs. These signals, following Fig. 4.3, indicates the emergence of highly concentrated Ni vapor plumes. After $T = 75$ μs, the LIF signal broadens and weakens, forming more diffused structures. This reflects a combination of continued evaporation at lower rates and diffusion of the nickel atoms away from the electrode surface. The relatively persistent signal up to around $T = 300$ μs indicates that the energy release by plasma remains sufficient to sustain evaporation for several hundred microseconds after breakdown. From $T = 400$ μs onward, the fluorescence intensity steadily diminishes.

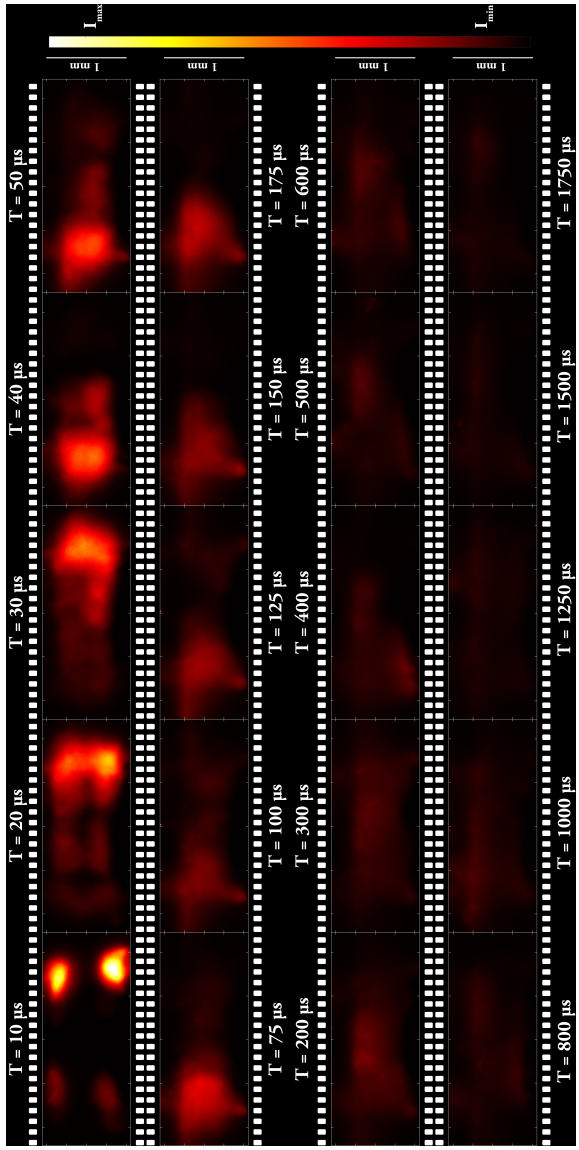

Figure 4.4: **Time-resolved laser-induced fluorescence images of nickel vapor at 6 bar ambient pressure.** Each frame represents the average of 100 spark events and corresponds to a specific delay time after the breakdown phase during a 3 ms DC spark discharge. The images show the distribution of nickel atoms within the 1 mm electrode gap of the spark plug. The cathode is located at the top, and the anode at the bottom.

These LIF images provide compelling visual evidence that thermal evaporation is a key driver of electrode material loss in spark discharges, especially under elevated pressure conditions. The prolonged presence of nickel vapor indicates that once formed, the hot spots on the electrode can sustain evaporation well beyond the initial breakdown.

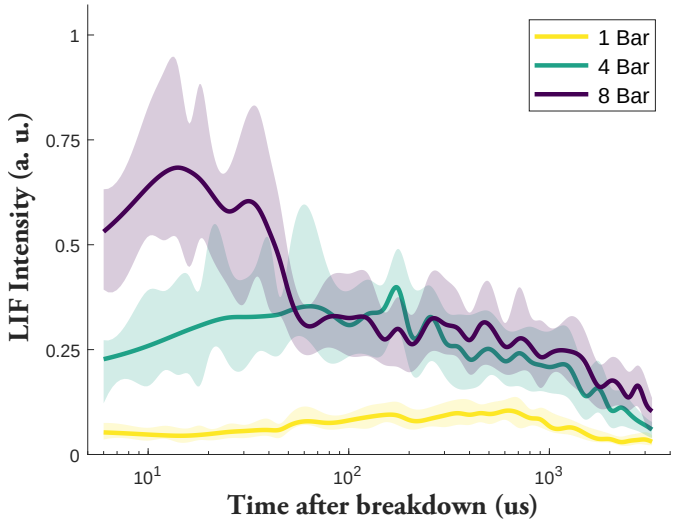

Figure 4.5: **Temporal evolution of LIF intensity after breakdown phase from 6 μs to 3250 μs for 3 ms DC sparks under different ambient pressures.**
Colored curves represent median-fitted profiles, while the shaded regions indicate the measurements variability.

4.3 Refinement of the evaporation model

DC sparks with a fixed 3 ms dwell time was investigated under different ambient pressures from 1 bar to 8 bar. Fig. 4.5 is the intensity of detected LIF signal at different time after breakdown during the spark discharge. Only representative data (1 bar, 4 bar and 8 bar) is presented in the plot. As the ambient pressure becomes higher, an increase in the LIF signal was observed, indicating a greater population of nickel atoms. However, an apparent contradiction of the fluorescence quantum yield arises when considering collisional quenching effects (Eq. 3.4) at elevated pressures. A higher density of colliding species under elevated pressure conditions should lead to an increased collisional quenching rate, which would result in a decrease in the LIF signal intensity due to more frequent deactivation of excited states. Hence, the actual nickel from the electrodes must be higher than the indicated LIF intensity with increasing pressure.

The dwell time of the the inductive coil was fixed at 3 ms, ensuring that the energy of DC sparks remained constant. According to Jones' evaporation model discussed in Section 2.3, this should result in comparable levels of electrode evaporation across all cases. However, this prediction clearly contradicts the LIF measurements considering that the only parameter varied was the ambient pressure and thus the breakdown voltage.

As defined in Section 2.2.1, the instantaneous power of the spark can be expressed as

$$P_{spark} = u \cdot i. \tag{4.1}$$

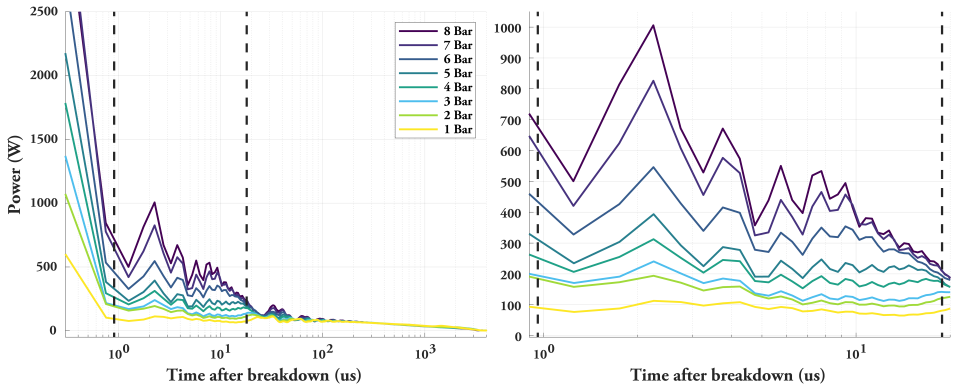

Figure 4.6: The power of DC sparks with the same energy at different ambient pressures.

Figure 4.6 shows the profiles of spark power under different pressures, where the total energy is held constant [4.2]. In comparison with the intensity of LIF signals in Fig. 4.5, it can be deducted that the power of spark plays a more dominant role in driving electrode evaporation than spark energy.

To further validate this finding, additional experiments were conducted, and the detailed results and discussion can be seen in **Paper IV**. Only the main conclusions are summarized here. DC sparks with varying energies were investigated under a constant ambient pressure. Sparks with lower energies yielded weaker LIF signals. This behavior is attributed to the shorter dwell times (i.e. lower energy), which lead to the reduced value of current and consequently lower spark power. To decouple the effects of spark energy and ambient pressure, AC sparks with controlled peak currents were also examined. The results showed that sparks with higher peak currents produced stronger LIF signals. These observations consistently support the conclusion that spark power, rather than total energy, is the dominant factor governing the detected nickel atoms in gas phase.

The evaporation model proposed by F.L. Jones treats a single spark event as creating hot spots on the electrodes. In essence, the spark deposits a certain energy W_{spark} into a tiny area of the electrode, and this energy is partitioned into two components: (i) the energy required to heat and vaporize a volume of metal (Eq. 2.6) and (ii) various losses (Eq. 2.2). The condition was assumed that the hot spots reach a steady temperature - the boiling temperature of the electrode material - during the discharge. In that state, any additional energy input goes into the evaporation of the metal electrodes. However, based on the discussions above, the author want to propose a refinement of this model, which in short, the spark power dominates the processes instead of the spark energy.

From Eq. 2.5, whether the temperature of hot spots T_t at time t will exceed the boiling

[4.2] The observed 'ringing' behavior arises from the resonant nature of the RLC circuit.

temperature T_b or not is decided by the spark power P_{spark} per unit area (S) and the spark duration t. Although the spark power during the breakdown phase can reach hundreds or even thousands of watts, its short duration is insufficient to heat the electrode material to the evaporation temperature. The nickel atoms observed in the gas phase within the spark plug gap originate from the sputtering process.

Although the total area of hot spots varies during discharges, its influence is negligible compared with that of the spark power [74, 99]. Thus, the minimum spark power required to sustain the evaporation can be estimated by modifying Eq. 2.2 to

$$P_{spark} = r + q, \tag{4.2}$$

if the electrode surfaces reach the boiling temperature. Combined with Eq. 2.3 and Eq. 2.4,

$$P_{spark} = \varepsilon\sigma S(T_b^4 - T^4) + 2k\sqrt{\pi S}(T_b - T). \tag{4.3}$$

Such a refinement of the evaporation model can provide an improved framework for interpreting the observed laser-induced fluorescence signal of nickel atoms.

Chapter V

Summary and outlook

You don't have to see the whole staircase,
just take the first step.

— Martin Luther King Jr.

In this thesis, laser-based optical methods was introduced for diagnostics of electrode wear for the first time. A comprehensive analysis of spark discharge used in SI-ICEs has been done. The voltage and current characterization and various mechanisms of spark-induced electrode wear at different phases were briefly overviewed. OES and LIF have been successful applied and ultilized to investigate the spark plug wear with nickel-based alloy electrodes.

OES measurements revealed the existence of nickel atoms and most of the observed emissions lie within the spectral region bewtween two nitrogen emission bands ($C \rightarrow B, \Delta v = 0, 1$). Excitation spectrum determines the most favorable transition for nickel is at 336.96 nm. The effective fluorescence lifetime was measured to be about 1.1 ns throughout the duration of the discharge at atmospheric condition.

A two-dimensional LIF was then successfully performed within the spark plug gap. Various parameters, such as breakdown voltage, coil energy, ambient pressure and gas composition, were examined to study how they can affect the wear process of the electrode. Different distributions of laser-induced nickel fluorescence within the spark plug gap indicate different mechanisms for the electrode wear. In low pressure, the wear comes from sputtering. While, under high pressure, the high current following the high breakdown voltage melts and boils the electrodes, causing the evaporation. The power of spark has been identified as the determining factor governing the balance between sustained evaporation and heat dissipation.

Overall, this thesis delivers a practical stragety as a cornerstone to perform laser diagnostics

on spark plug wear. New insights are also provided to advance the understanding of spark-induced electrode wear.

Outlook

The understanding of the wear mechanisms is not only valuable for academia, but also can help the industry optimize the ignition systems and spark plug materials that can achieve the twin goals of reliable ignition and long life of the electrodes. Thus, further research remains needed to investigate the interactions between spark discharges and the electrodes.

This thesis was conducted specifically with nickel electrodes, the applicability of the LIF technique can extend far beyond this material and setup. The strategy can also be applied to spark plugs made of other metals, such as platinum (Pt) and iridium (Ir). Also, due to the limitation of the lab-scale test rig, more parameters that are relevant for evaporation process were untested, for example, the temperature of the electrode. With more information, my refinement of Jones' evaporation model could be further validated.

The output of the thesis is based on 'quasi-single' spark measurements. High repetition-rate burst mode laser together with OPO would be a better choice towards single spark diagnostics. Such excitation source could be highly interesting for revealing the dynamics during one single spark discharge. Another limitation is the qualitative LIF data, primarily due to insufficient knowledge. Further data about the population distributions among energy levels and the fluorescence lifetimes under varying ambient pressures may enable a transition towards quantitative measurements.

Based on other proposed wear mechansims, other laser-based optical diagnostics could be performed, for example, detection of particle ejection with laser-induced Mie scattering and oxides with Raman scattering.

These ideas can be considered as a guidance and explored further. Together with long-term test results in real engine environment, the understanding of electrode wear will be more deepened. In all, the ultimate goal is to build a theoretical model to describe the spark-induced electrode wear.

References

[1] S. Chu and A. Majumdar. Opportunities and challenges for a sustainable energy future. *Nature*, 488(7411):294–303, August 2012.

[2] J. Davenport and N. Wayth. *Statistical Review of World Energy 2024*. Energy Institute, 73rd edition, 2024.

[3] IEA. World Energy Outlook 2021. Technical report, International Energy Agency, October 2021.

[4] IEA. World Energy Outlook 2022. Technical report, International Energy Agency, October 2022.

[5] IEA. World Energy Outlook 2023. Technical report, International Energy Agency, October 2023.

[6] IEA. World Energy Outlook 2024. Technical report, International Energy Agency, October 2024.

[7] IEA. Energy Policy Review Sweden 2024. Technical report, International Energy Agency, November 2024.

[8] Eurostat. Shedding light on energy in Europe - 2025 edition. *Shedding light on energy in Europe*, 2025.

[9] H. Khatib, A. Barnes, I. Chalabi, H. Steeg, and K. Yokobori. Chapter 4 - Energy Security. *World Energy Assessment: Energy and the Challenge of Sustainability*, November 2025.

[10] G. Pirker and A. Wimmer. Sustainable power generation with large gas engines. *Energy Conversion and Management*, 149:1048–1065, October 2017. Publisher: Elsevier BV.

[11] H. Kobayashi, A. Hayakawa, K.D.K.A. Somarathne, and E.C. Okafor. Science and technology of ammonia combustion. *Proceedings of the Combustion Institute*, 37(1):109–133, 2019.

[12] G.A. Karim. Hydrogen as a spark ignition engine fuel. *International Journal of Hydrogen Energy*, 28(5):569–577, May 2003.

[13] S. Verhelst and T. Wallner. Hydrogen-fueled internal combustion engines. *Progress in Energy and Combustion Science*, 35(6):490–527, December 2009.

[14] J. Ängeby, A. Saha, O. Björnsson, and M. Lundgren. Spark Ignition - Searching for the Optimal Spark Profile. In *9th International Engine Congress 2022*, Baden Baden, Germany, February 2022.

[15] S.H. Hosseini, A. Tsolakis, A. Alagumalai, O. Mahian, S.S. Lam, J. Pan, W. Peng, M. Tabatabaei, and M. Aghbashlo. Use of hydrogen in dual-fuel diesel engines. *Progress in Energy and Combustion Science*, 98:101100, September 2023.

[16] J. Ängeby, J. Tidholm, B. Gustafsson, and A. Johnsson. Ignition Systems for SI-ICE Fueled by Alternative and Renewable Fuels. In *ASME 2023 ICE Forward Conference*, page V001T03A005, Pittsburgh, Pennsylvania, USA, October 2023. American Society of Mechanical Engineers.

[17] IPCC. *Global Warming of 1.5°C: IPCC Special Report on Impacts of Global Warming of 1.5°C above Pre-industrial Levels in Context of Strengthening Response to Climate Change, Sustainable Development, and Efforts to Eradicate Poverty*. Cambridge University Press, 1st edition, June 2022.

[18] UNFCCC. COP28 The UAE Consensus, December 2023.

[19] H.M. Cho and B.-Q. He. Spark ignition natural gas engines—A review. *Energy Conversion and Management*, 48(2):608–618, February 2007.

[20] P. Dimitriou and T. Tsujimura. A review of hydrogen as a compression ignition engine fuel. *International Journal of Hydrogen Energy*, 42(38):24470–24486, September 2017.

[21] O.I. Awad, R. Mamat, O.M. Ali, N.A.C. Sidik, T. Yusaf, K. Kadirgama, and M. Kettner. Alcohol and ether as alternative fuels in spark ignition engine: A review. *Renewable and Sustainable Energy Reviews*, 82(3):2586–2605, February 2018.

[22] S.K. Mahendar, A. Erlandsson, and L. Adlercreutz. Challenges for Spark Ignition Engines in Heavy Duty Application: a Review. In *SAE Technical Paper*, pages 2018–01–0907, US, April 2018. SAE International. Automotive, Commercial Vehicle.

[23] H. Levinsky. Why can't we just burn hydrogen? Challenges when changing fuels in an existing infrastructure. *Progress in Energy and Combustion Science*, 84:100907, May 2021.

[24] A. Tilz, C. Kiesling, G. Meyer, A. Nickl, G. Pirker, and A. Wimmer. Experimental investigation of the influence of ignition system parameters on combustion behavior in large lean burn spark ignited gas engines. *Experimental Thermal and Fluid Science*, 119:110176, November 2020.

[25] A. Tilz, C. Kiesling, G. Pirker, and A. Wimmer. Influence of initial electric arc root position on electric arc behavior with spark plugs in large lean burn spark ignited gas engines. *International Journal of Engine Research*, page 14680874241236512, March 2024.

[26] M. Weinrotter, H. Kopecek, E. Wintner, M. Lackner, and F. Winter. Application of laser ignition to hydrogen-air mixtures at high pressures. *International Journal of Hydrogen Energy*, 30(3):319–326, March 2005.

[27] J. Ängeby, B. Gustafsson, and A. Johnsson. Ignition Control Module for Hydrogen Combustion Engines. *MTZ Worldwide*, 84:48–53, September 2023.

[28] H. Albrecht, W.H. Bloss, W. Herden, R. Maly, B. Saggau, and E. Wagner. New Aspects on Spark Ignition. In *SAE Technical Paper*, page 770853, US, February 1977. SAE International.

[29] M.L. Jeswani. Roughness and wear characteristics of spark-eroded surfaces. *Wear*, 51(2):227–236, December 1978.

[30] D. Nakano, T. Suzuki, and M. Matsui. Gas Engine Ignition System for Long-Life Spark Plugs. In *SAE Technical Paper*, pages 2004–32–0086, US, September 2004. SAE International. Automotive.

[31] Y. Shimanokami, Y. Matsubara, T. Suzuki, and W. Matsutani. Development of High Ignitability with Small Size Spark Plug. In *SAE Technical Paper*, pages 2004–01–0987, US, March 2004.

[32] H.T. Lin, M.P. Brady, R.K. Richards, and D.M. Layton. Characterization of erosion and failure processes of spark plugs after field service in natural gas engines. *Wear*, 259(7-12):1063–1067, July 2005.

[33] S. Nishioka, K. Hanashi, and S. Okabe. Super Ignition Spark Plug with Wear Resistive Electrode. In *SAE Technical Paper*, pages 2008–01–0092, US, April 2008. SAE International. Automotive.

[34] S. Javan, S.V. Hosseini, and S.Sh. Alaviyoun. An experimental investigation of spark plug temperature in bi-fuel engine and its effect on electrode erosion. *International Journal of Automotive Engineering*, 2(1):21–29, January 2012.

[35] S. Javan, S.V. Hosseini, S.Sh. Alaviyoun, and F. Ommi. Effect of electrode erosion on the required ignition voltage of spark plug in CNG spark ignition engine. *The Journal of Engine Research*, 26(26):31–39, November 2012.

[36] S. Javan, S.Sh. Alaviyoun, S.V. Hosseini, and F. Ommi. Experimental study of fine center electrode spark plug in bi-fuel engines. *Journal of Mechanical Science and Technology*, 28(3):1089–1097, March 2014.

[37] F. Fernandes, M. Lönarz, and P. Weyand. Development of an Ignition Coil Integrated System to Monitor the Spark Plugs Wear. In M. Günther and M. Sens, editors, *Ignition Systems for Gasoline Engines*, pages 140–151. Springer International Publishing, Cham, 2017.

[38] S. Różowicz. Use of the mathematical model of the ignition system to analyze the spark discharge, including the destruction of spark plug electrodes. *Open Physics*, 16(1):57–62, March 2018.

[39] D. Scherjau, G. Meyer, J. Rosc, Th. Mai, A. Gschirr, and A. Wimmer. Erosion processes of electrodes –Experiments and modeling. *Wear*, 428-429:85–92, June 2019.

[40] C. Tambasco, M. Hall, and R. Matthews. Effects of Spark Plug Operating Conditions on Electrode Erosion and Surface Deformation. In *SAE Technical Paper*, Detroit, Michigan, United States, April 2024. SAE International. ISSN: 0148-7191, 2688-3627.

[41] E.M. Bazeljan and Y.P. Raizer. *Spark discharge*. CRC Press, Boca Raton, Fla. New York, NY, 1998.

[42] D.R. Crosley. Laser-induced fluorescence in spectroscopy, dynamics, and diagnostics. *Journal of Chemical Education*, 59(6):446, June 1982.

[43] J.W. Daily. Laser induced fluorescence spectroscopy in flames. *Progress in Energy and Combustion Science*, 23(2):133–199, 1997.

[44] J. Amorim, G. Baravian, and J. Jolly. Laser-induced resonance fluorescence as a diagnostic technique in non-thermal equilibrium plasmas. *Journal of Physics D: Applied Physics*, 33(9):R51–R65, May 2000.

[45] M. Aldén, J. Bood, Z. Li, and M. Richter. Visualization and understanding of combustion processes using spatially and temporally resolved laser diagnostic techniques. *Proceedings of the Combustion Institute*, 33(1):69–97, 2011.

[46] E.V. Barnat. Multi-dimensional optical and laser-based diagnostics of low-temperature ionized plasma discharges. *Plasma Sources Science and Technology*, 20(5):053001, September 2011.

[47] Y. Bao, K. Dorozynska, P. Stamatoglou, C. Kong, T. Hurtig, S. Pfaff, J. Zetterberg, M. Richter, E. Kristensson, and A. Ehn. Single-shot 3D imaging of hydroxyl radicals in the vicinity of a gliding arc discharge. *Plasma Sources Science and Technology*, 30(4):04LT04, April 2021.

[48] M. Aldén. Spatially and temporally resolved laser/optical diagnostics of combustion processes: From fundamentals to practical applications. *Proceedings of the Combustion Institute*, 39(1):1185–1228, 2023.

[49] Y. Bao, K. Zhang, J. Sun, T. Hurtig, A.A. Konnov, M. Richter, E. Kristensson, and A. Ehn. A comprehensive study on dynamics of flames in a nanosecond pulsed discharge. Part I: Discharge formation and gas heating. *Combustion and Flame*, 275:114075, May 2025.

[50] J. Sun, Y. Bao, K. Zhang, A.A. Konnov, M. Richter, E. Kristensson, and A. Ehn. A comprehensive study on dynamics of flames in a nanosecond pulsed discharge. Part II: Plasma-assisted ammonia and methane combustion. *Combustion and Flame*, 275:114076, May 2025.

[51] R. Maly. Spark Ignition: Its Physics and Effect on the Internal Combustion Engine. In J.C. Hilliard and G.S. Springer, editors, *Fuel Economy*, pages 91–148. Springer US, Boston, MA, 1 edition, 1984. Subtitle: in Road Vehicles Powered by Spark Ignition Engines.

[52] Y.P. Raizer. *Gas Discharge Physics*. Springer-Verlag, Berlin, Heidelberg, 1987.

[53] S. Huang, T. Li, P. Ma, S. Xie, Z. Zhang, and R. Chen. Quantitative evaluation of the breakdown process of spark discharge for spark-ignition engines. *Journal of Physics D: Applied Physics*, 53(4):045501, January 2020.

[54] A. Anders. Glows, arcs, ohmic discharges: An electrode-centered review on discharge modes and the transitions between them. *Applied Physics Reviews*, 11(3):031310, September 2024.

[55] N. Jeanvoine, R. Jonsson, and F. Muecklich. Investigation of the arc and glow phase fractions of ignition discharges in air and nitrogen for Ag, Pt, Cu and Ni electrodes. In *Proceedings of XXVIII International Conference on Phenomena in Ionized Gases*, pages 284–287, Prague, Czech Republic, July 2007. Institute of Plasma Physics AS CR. https://iopscience.iop.org/article/10.1088/0963-0252/17/2/020201 https://plasma.karelia.ru/events/info/ICPIG2007.pdf.

[56] B. Miedziński, G. Wiśniewski, S.N. Kharin, and H. Nouri. Possibility of Control of Transition of Switching Arc Dc into Glowing. *Proceedings of the Pakistan Academy of Sciences*, 49(3):173–180, September 2012.

[57] J.F. Griffiths and J.A. Barnard. *Flame and Combustion*. Springer Netherlands, Dordrecht, 1995.

[58] S. Shy. Spark ignition transitions in premixed turbulent combustion. *Progress in Energy and Combustion Science*, 98:101099, September 2023.

[59] J.D. Dale, M.D. Checkel, and P.R. Smy. Application of high energy ignition systems to engines. *Progress in Energy and Combustion Science*, 23(5-6):379–398, 1997.

[60] K. Nishio, T. Oshima, and H. Ogura. A study on spark plug electrode shape. *International Journal of Vehicle Design*, 15(1/2):119–130, 1994.

[61] B.N. Chapman. *Glow Discharge Processes: Sputtering and Plasma Etching*. Wiley & Sons Ltd, New York, November 1980.

[62] J.A. Rich. Resistance Heating in the Arc Cathode Spot Zone. *Journal of Applied Physics*, 32(6):1023–1031, June 1961.

[63] F.A. Soldera, F.T. Mucklich, K. Hrastnik, and T. Kaiser. Description of the Discharge Process in Spark Plugs and its Correlation With the Electrode Erosion Patterns. *IEEE Transactions on Vehicular Technology*, 53(4):1257–1265, July 2004.

[64] J.L. Vossen, S. Krommenhoek, and V.A. Koss. Some experiments that provide direct visualization of reactive sputtering phenomena. *Journal of Vacuum Science & Technology A: Vacuum, Surfaces, and Films*, 9(3):600–603, May 1991.

[65] H.C. Miller. Vacuum Arc Anode Phenomena. *IEEE Transactions on Plasma Science*, 5(3):181–196, 1977.

[66] M. Van Straaten, R. Gijbels, F.G. Melchers, H. Beske, and K. Swenters. Atomization phenomena of metals in a d.c.-spark vacuum discharge. *International Journal of Mass Spectrometry and Ion Processes*, 93(2):125–140, October 1989.

[67] A.I. Karlina, A.E. Balanovskiy, V.V. Kondratiev, V.V. Romanova, A.G. Batukhtin, and Y.I. Karlina. An Investigation into the Behavior of Cathode and Anode Spots in a Welding Discharge. *Applied Sciences*, 14(21):9774, October 2024.

[68] E.A. Litvinov. Theory of Explosive Electron Emission. *IEEE Transactions on Electrical Insulation*, EI-20(4):683–689, August 1985. Publisher: Institute of Electrical and Electronics Engineers (IEEE).

[69] P. Sigmund. Theory of Sputtering. I. Sputtering Yield of Amorphous and Polycrystalline Targets. *Physical Review*, 184(2):383–416, August 1969.

[70] P. Sigmund, A. Oliva, and G. Falcone. Sputtering of multicomponent materials: Elements of a theory. *Nuclear Instruments and Methods in Physics Research*, 194(1-3):541–548, March 1982.

[71] R. Kelly and D.E. Harrison. A summary of the theory of the preferential sputtering of alloys. *Materials Science and Engineering*, 69(2):449–455, March 1985.

[72] Y. Yamamura, N. Matsunami, and N. Itoh. Theoretical studies on an empirical formula for sputtering yield at normal incidence. *Radiation Effects*, 71(1-2):65–86, January 1983. Publisher: Informa UK Limited.

[73] F. Llewellyn-Jones. Electrode Evaporation and the Electric Spark. *Nature*, 157:298–299, March 1946.

[74] F. Llewellyn-Jones. Electrode Erosion by Spark Discharges. *British Journal of Applied Physics*, 1(3):60–65, March 1950.

[75] F. Llewellyn-Jones. The Mechanism of Electrode Erosion in Electrical Discharges: Physical Basis of the Low Erosion Rate of the Platinum Metals. *Platinum Metals Review*, 7(2):58–65, April 1963.

[76] E.W. Gray, J.A. Augis, and F.J. Gibson. Plasma and electrode interactions in short gap discharges in air I. Plasma effects†. *International Journal of Electronics*, 30(4):301–313, April 1971.

[77] J.A. Augis, F.J. Gibson, and E.W. Gray. Plasma and electrode interactions in short gap discharges in air II. Electrode effects†. *International Journal of Electronics*, 30(4):315–332, April 1971.

[78] E.W. Gray and J.R. Pharney. Electrode erosion by particle ejection in low-current arcs. *Journal of Applied Physics*, 45(2):667–671, February 1974.

[79] C.T. Young and D.A. Grimes. Erosion Mechanisms of Automotive Spark Plug Electrodes. In *SAE Technical Paper*, page 780330, US, February 1978. SAE International. Automotive.

[80] J. Rager, A. Flaig, G. Schneider, T. Kaiser, F. Soldera, and F. Mücklich. Oxidation Damage of Spark Plug Electrodes. *Advanced Engineering Materials*, 7(7):633–640, July 2005.

[81] J. Rager, J. Böhm, T. Kaiser, A. Flaig, and F. Mücklich. Design and Materials for Long-Life Spark Plugs. In *SAE Technical Paper*, pages 2006–01–0617, US, April 2006. SAE International. Automotive.

[82] S. Svanberg. *Atomic and molecular spectroscopy: basic aspects and practical applications*. Advanced texts in physics. Springer, Berlin ; New York, 4th, rev. ed edition, 2004.

[83] C.J. Foot. *Atomic physics*. Number 7. Atomic, Optical, and laser physics in Oxford master series in physics. Oxford University Press, Oxford ; New York, 2005.

[84] A. Kramida, Yu. Ralchenko, J. Reader, and NIST ASD Team (2024). NIST Atomic Spectra Database (ver. 5.12), [Online], February 2025.

[85] W. Demtröder. *Atoms, Molecules and Photons: An Introduction to Atomic-, Molecular- and Quantum Physics*. Graduate Texts in Physics. Springer Berlin Heidelberg, Berlin, Heidelberg, 2010. ISSN: 1868-4513, 1868-4521.

[86] D.R. Demers and C.D. Allemand. Atomic fluorescence spectrometry with an inductively coupled plasma as atomization cell and pulsed hollow cathode lamps for excitation. *Analytical Chemistry*, 53(12):1915–1921, October 1981.

[87] J.B. Simeonsson, K.C. Ng, and J.D. Winefordner. Single- and Double-Resonance Atomic Fluorescence Spectrometry with Inductively Coupled Plasma Atomization and Laser Excitation. *Applied Spectroscopy*, 45(9):1456–1462, November 1991.

[88] J.W. Olesik. Fundamental Research in ICP-OES and ICPMS. *Analytical Chemistry*, 68(15):469–474, August 1996.

[89] S.E. Hobbs and J.W. Olesik. The influence of incompletely desolvated droplets and vaporizing particles on chemical matrix effects in inductively coupled plasma spectrometry: time-gated optical emission and laser-induced fluorescence measurements. *Spectrochimica Acta Part B: Atomic Spectroscopy*, 52(3):353–367, March 1997.

[90] A.C. Eckbreth. *Laser Diagnostics for Combustion Temperature and Species*, volume 3 of *Combustion Science & Technology Book Series*. CRC Press, London, 2 edition, 1996.

[91] A.E. Siegman. *Lasers*. Univeristy Science Books, Mill Valley, California, 1986.

[92] R. Schnabel and M. Kock. Time-resolved nonlinear laser-induced fluorescence technique for a combined lifetime and branching-fraction measurement. *Physical Review A*, 63(1):012519, December 2000.

[93] K.J.R. Weiland, M.L. Wise, and G.P. Smith. Laser-induced fluorescence detection strategies for sodium atoms and compounds in high-pressure combustors. *Applied Optics*, 32(21):4066, July 1993.

[94] J. Heldt, H. Figger, K. Siomos, and H. Walther. Lifetime Measurements of Some Levels Belonging to the $3d^8\ 4s(a^2\ F)\ 4p$ Configuration of Ni I. *Astronomy and Astrophysics*, 39:371–375, March 1975.

[95] U. Becker, H. Kerkhoff, M. Schmidt, and P. Zimmermann. A test of the absolute Ni(I) *gf* -value scale by using mean lives of selected levels for the configurations $3d^8\ 4s4p$ and

$3d^9\,4p$. *Journal of Quantitative Spectroscopy and Radiative Transfer*, 25(4):339–343, April 1981.

[96] D.E. Blackwell, A.J. Booth, A.D. Petford, and J.M. Laming. Measurement of relative oscillator strengths for Ni I. Transitions from levels $a^3F_{4\text{-}2}$ (0.00-0.27 eV), $a^3D_{3\text{-}1}$ (0.03-0.21 eV) and a^1D_2 (0.42 eV). *Monthly Notices of the Royal Astronomical Society*, 236(2):235–245, January 1989.

[97] S.D. Bergeson and J.E. Lawler. Radiative lifetimes in Ni I. *Journal of the Optical Society of America B*, 10(5):794, May 1993.

[98] A. Ehn, O. Johansson, J. Bood, A. Arvidsson, B. Li, and M. Aldén. Fluorescence lifetime imaging in a flame. *Proceedings of the Combustion Institute*, 33(1):807–813, 2011. Publisher: Elsevier BV.

[99] F. Soldera, A. Lasagni, F. Mücklich, T. Kaiser, and K. Hrastnik. Determination of the cathode erosion and temperature for the phases of high voltage discharges using FEM simulations. *Computational Materials Science*, 32(1):123–139, January 2005. Publisher: Elsevier BV.

Acknowledgements

'Part of the journey is the end.'

When looking back throughout my Ph.D. careeer, I thought finding the signal was difficult when I started working on this project. After finishing the alignment, I thought optimizing the signal was difficult when I planned to start the measurements. After fixing damaged equipment, I thought telling a publishable story was difficult when I was taking data. After submitting the manuscript, I thought getting accepted was difficult when the feedbacks came back from the reviewers. After receiving the decision of acceptance, I thought applying for some fundings to go further was difficult when I drafted my first proposal. Closing to the finish, I thought such infinite loop was difficult when I was writing this thesis. However, after 1675 days, although I do still feel confused sometimes, I will not be afraid in the next chapter of my life because this journey was accompanied by all of you.

Mattias. During the first kick-off meeting of LTH Profile Area *The Energy Transistion*, the host asked all participants what your competence is for this field and my answer was, 'Mattias is my supervisor!'. Till now, my answer remains the same. Although most of the time I prefer to explore slowly by myself, you always trust me and be extremely patient. Your understanding when I escaped from the lab and encouragement when I lost my confidence will forever be my treasure.

Andreas. Your office was always the first place I was heading to when I met any problems. You are always willing to help and answer my 'stupid' and 'childish' questions. Your passion and attitude for work will always guide me. The week we spent for the conference in German and those late nights and weekends we stayed in the division will definitely be my lifelong memories.

Jakob. Now, I finally feel and understand *'No Pressure'* you were always saying. Those large amount of meetings we had during the years are always funny and valuable. Your curiousity and ambition trying to understand the physics behind this project definitely inspired and pushed us towards the truth a lot.

Mattias group. The weekly group meeting was always a pleasure time. **Henrik**, your professional and responsible attitude will always be a model for me. **David S.**, your optimistic and positive thinking makes me ease all the time. I will remember our happy time on the slopes, probably also the cracked rib. **Saeed**, our conversations and football time were never boring and for sure, Hala Madrid! **Giota** & **Ruike**, the days we spent together in the lab were absolutely a wonderful memory. **Sebastian**, thanks for all the help which you are always willing to. **Aravind**, I have to say that sometimes I enjoyed the suffering we had in the same time, which made me never feel alone. Without me, you will surely have all the best luck in the lab! **Megha**, you were like my non-official office mate. It felt heartwarming everytime talking to you. **Jan-Peter**, our belly greeting and limited office-sharing time were funny. **Praja**, when you became like that dude in Mumbai, we will not need to fix any broken crystals and other stuff, although it was a good time.

Yupan, we experienced so many things together, not only work-wise, but also in life. The folder *Yupan's_Torture* tells all and will definitely tell more. **Christian**, thanks for your unreserved knowledge about the dye laser systems. Those days were wonderful when we fixed the lasers together, not only I gained a lot from your experience, but also those were several days I had company in the lab. **Igor**, unlike the photons I play with, you deal with the electrons. Thanks for all the knowledge about circuit learnt in your studio! **Jinguo**, even though I am not willing to admit, I really learnt a lot from you about how to perform a research systematically. Those days and nights in the plasma lab were always interesting although I still can not fully get your sense of humor.

The peers, **Zhiyong**, **Yue Q.** and **Jundie**, the moments we had together were full of laughter and fun. **Shen**, **Wubin**, **Can** and **Niklas**, your experiences and understanding about research helps me along these years. **David F.**, the best office neighbor and teammate! **Lisa** and **Saga**, the running we did in the heavy rain along the Charles River was wild. **Alsu** and **Maria**, the jokes we made and the slopes we ran were such great memories. **Vassily**, thanks for the 'Bible'! I will have no worries about the FRAME technique. **Robin**, those politically-incorrect talk we had in the office hopefully will never come out of E423. **Sam**, thanks for involving me in your experiments! It is so interesting to perform measurements from a 'reverse' direction. Please take care of the laser!

Minna, **Cecilia**, **Edward**, **Elias**, **Joakim**, **Meena**, **Alexander**, **Johan F.**, **Meng** and **Sven-Inge**, all the unconscious help you did will always stay in my heart. Also, I want to thank the guest researchers, **Jianqing**, **Zihao S.**, **Siyu**, **Qi**, **Qianjin**, **Xianzhong**, **Zhaomin**, **Liwei**, **Weilun**, **Weitian**, **Jibiao** and **Xiaomin**, for all the good time we had together.

Xin, **Qingshuang** and **Yingzhe**, it was so lucky for me that my time in Lund was accompanied by you. Huge loooove and thanks! **Huaiyu**, it is nice to have you as the neighbor! One day, we will speak with joy with wine in our hands.

My bros, **Jinchen**, **Xuecheng**, **Yubiao**, **Qiang**, **Hong**, **Weibo**, **Zihao T.** and **Lujie**, the

youthful and frivolous days will always be one of my happiest time. **Fangliu** and **Shiyuan**, our journey in Iceland was such an unique memory and hopefully will not happen again. My sis **Yi**, all the alcohol we drank and all the arguments we had will bond us from the past to the future.

Special thanks given to my partner **Yue Z.** in every aspect. From universe to philosophy, from U. S. to Europe, all the discussions and trips we had together will consist part of me, no matter what.

最后，感谢父母无条件的爱和支持。自记事起，我从来都不是一个老师们眼中的“好”孩子，谢谢你们一直以来的包容与培养。此外，作为前辈，我也从你们身上学到了许多做人做事的道理。

Appendix

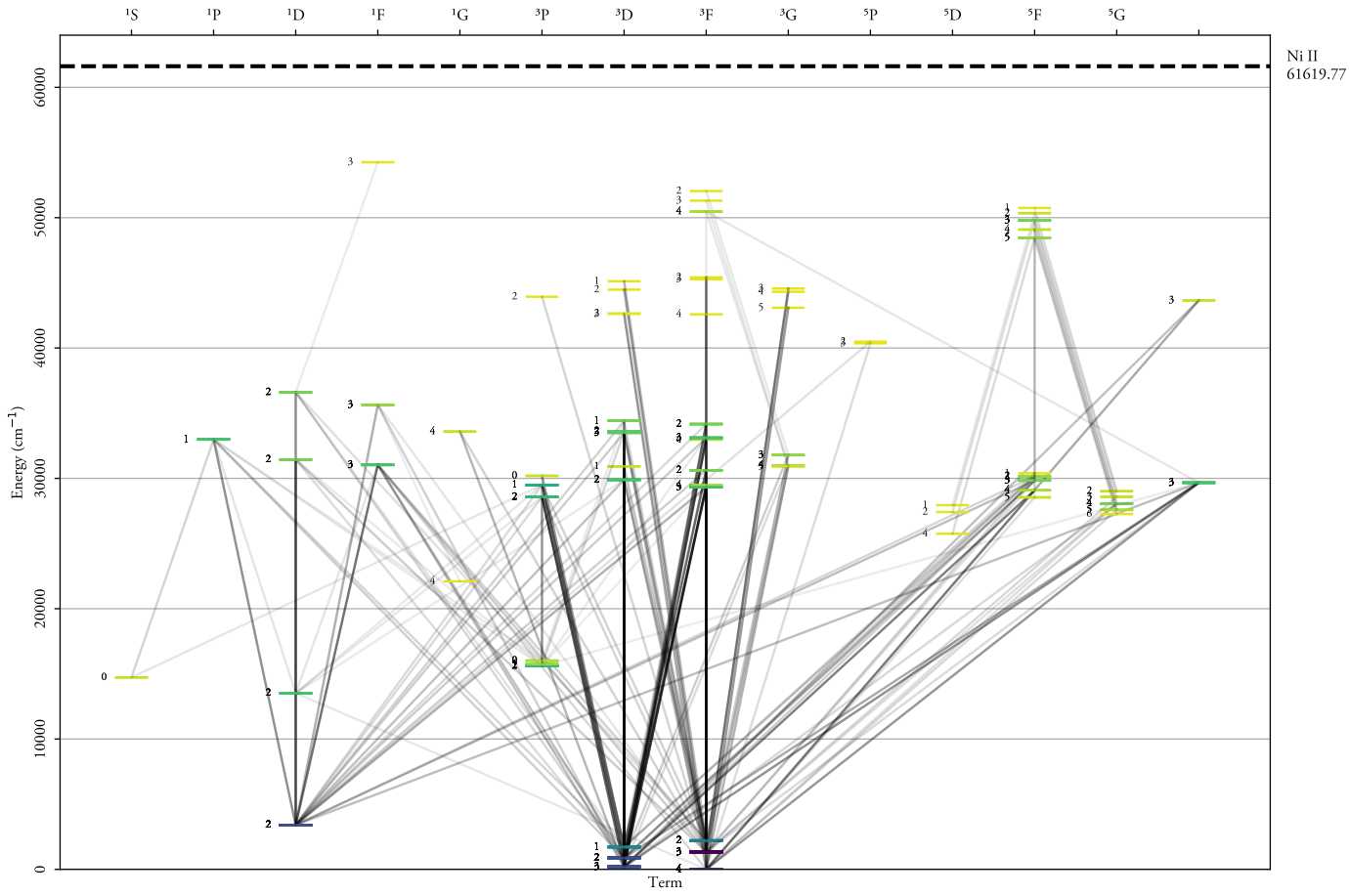

Figure A.1: **Grotrian diagram of neutral nickel atom (Ni-I), which is plotted based on the open source data in NIST Atomic Spectra Database.** The figure is to show the 'sea' of energy levels and lines.

Research Papers

Summaries and Author Contributions

Mentioned co-authors are abbreviated as follows:
Ruike Bi (R. Bi), Jakob Ängeby (Jakob).

Paper I:
Detection of Nickel Atoms Released from Electrodes in Spark Discharges Using Laser-Induced Fluorescence

The idea for this paper is to study the spectra of neutral nickel atoms generated by spark discharges, both on the emission and the excitation sides. Most plasma-induced nickel emission were found within a 'spectral window' between 339 nm and 354 nm, between two strong nitrogen emission bands, which are suitable for nickel detection under intense plasma background. Following this, an excitation scan was performed using a tunable picosecond laser and the optimum excitation wavelength of 336.96 nm was found by studying the intensity of the emission spectra within this 'window', which can be used for performing 2D PLIF imaging measurements.

R. Bi and I designed the experiment and performed the measurements together. I did the data analysis and wrote the manuscript. All co-authors reviewed the manuscript and provided their feedbacks.

Paper II:
Effective lifetime of Ni laser induced fluorescence excited at 336.9 nm during spark plug discharge

Following Paper I, the idea of this paper is to measure the effective fluorescence lifetime of Ni atoms excited by a 336.96 nm laser in atmospheric conditions. The results indicated that the measured lifetime was constant around 1.1 ns during the whole spark discharge. Based on this, a linear correlation was found between the number density of Ni atoms and the detected LIF intensity. Using the conclusion above, the generation of Ni by DC discharges was studies temporally, showing that the number density maximize around 350 μs after gas breakdown, and decrease as the discharge continues.

R. Bi and I designed the experiment and performed the measurements together. I assisted in drawing figures and writing the manuscript. All co-authors reviewed the manuscript and provided their feedbacks.

Paper III:
Robust Ignition and Sparkplug Wear for H_2 SI-ICE

The aim of this proceeding paper is trying to give a brief review of spark discharges for ignition of SI-ICE and theoretical models for spark-induced electrode wear. Long-term test were performed and indicated that measurement methodology with a high temporal resolution is needed to reveal the mechanisms of the interaction between spark and electrode of sparkplug. Based on the previous two journal papers, prelinminary PLIF images show great compentence of such technique for further meansurements, by giving a spatial distribution of gas phase nickel atoms originated from electrodes.

I did the literature review about sparkplug wear and perform the PLIF experiments. Jakob and I wrote the manuscript together and I was responsible for the said sections. All co-authors reviewed the manuscript and provided their feedbacks.

Paper IV:
Investigation of Electrode Wear during Spark Discharges using Planar Laser-induced Fluorescence

The idea of the paper is to extend the PLIF measurements of sparkplug wear to a 'close-to-reality' condition with elevated pressures and an added cross-flow. Pressure was changed from 1 bar to 8 bars and different mechanisms were found for the existence of nickel within the 1 mm gap by comparing the spatial distribution. The temporal dynamics of evoparated nickel was studied. Two different types of spark discharge were examined, DC sparks with different dwell times and AC sparks with different peak currents. In the end, a pure nitrogen condition was compared with the air condition to study the impact of oxygen.

I designed the experiment and performed the measurements. I did the data analysis and wrote the manuscript. All co-authors reviewed the manuscript and provided their feedbacks.

inted by Media-Tryck, Lund 2025 NORDIC SWAN ECOLABEL 3041 0903

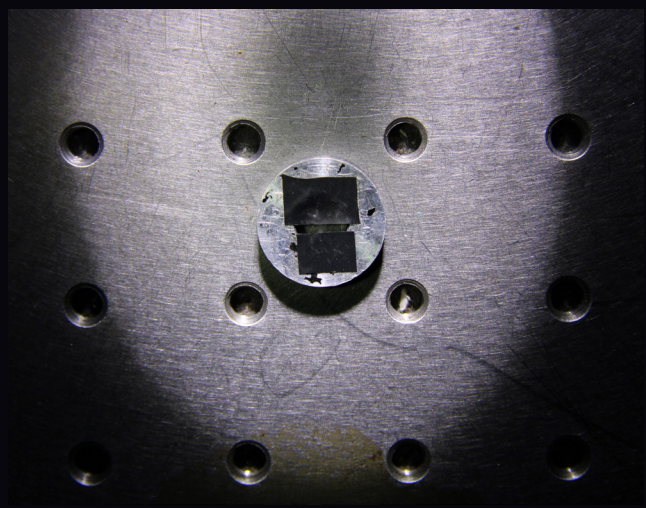

‘Salvation lay between’

LUND UNIVERSITY

Faculty of Engineering
Department of Physics
Division of Combustion Physics

ISBN 978-91-8104-507-9